2016

The age of three Middle Palaeolithic sites: single-grain optically stimulated luminescence chronologies for Pech de l'Azé I, II and IV in France

Zenobia Jacobs
University of Wollongong, zenobia@uow.edu.au

Nathan Jankowski
University of Wollongong, nrj934@uowmail.edu.au

Harold L. Dibble
Arizona State University, hdibble@upenn.edu

Paul Goldberg
University of Wollongong, goldberg@uow.edu.au

Shannon P. McPherron
Max Planck Institute for Evolutionary Anthropology, mcpherron@eva.mpg.de

See next page for additional authors

Publication Details

Jacobs, Z., Jankowski, N. R., Dibble, H. L., Goldberg, P., McPherron, S. J. P., Sandgathe, D. & Soressi, M. (2016). The age of three Middle Palaeolithic sites: single-grain optically stimulated luminescence chronologies for Pech de l'Azé I, II and IV in France. Journal of Human Evolution, 95 80-103.

The age of three Middle Palaeolithic sites: single-grain optically stimulated luminescence chronologies for Pech de l'Azé I, II and IV in France

Abstract
Optically stimulated luminescence (OSL) measurements were made on individual, sand-sized grains of quartz from Middle Palaeolithic deposits at three sites (Pech de l'Azé I, II and IV) located close to one another in the Dordogne region of southwest France. We were able to calculate OSL ages for 69 samples collected from these three sites. These ages reveal periods of occupation between about 180 and 50 thousand years ago. Our single-grain OSL chronologies largely support previous age estimates obtained by thermoluminescence dating of burnt flints at Pech IV, electron spin resonance dating of tooth enamel at Pech I, II and IV and radiocarbon dating of bone at Pech I and IV, but provide a more complete picture due to the ubiquitous presence of sand-sized quartz grains used in OSL dating. These complete chronologies for the three sites have allowed us to compare the single-grain ages for similar lithic assemblages among the three sites, to test the correlations among them previously proposed by Bordes in the 1970s, and to construct our own correlative chronological framework for the three sites. This shows that similar lithic assemblages occur at around the same time, and that where a lithic assemblage is unique to one or found at two of the Pech sites, there are no deposits of chronologically equivalent age at the other Pech site(s). We interpret this to mean that, at least for these Pech de l'Azé sites, the Mousterian variants show temporal ordering. Whether or not this conclusion applies to the wider region and beyond, the hypothesis that Mousterian industrial variation is temporally ordered cannot be refuted at this time.

Disciplines
Medicine and Health Sciences | Social and Behavioral Sciences

Publication Details
Jacobs, Z., Jankowski, N. R., Dibble, H. L., Goldberg, P., McPherron, S. J. P., Sandgathe, D. & Soressi, M. (2016). The age of three Middle Palaeolithic sites: single-grain optically stimulated luminescence chronologies for Pech de l'Azé I, II and IV in France. Journal of Human Evolution, 95 80-103.

Authors
Zenobia Jacobs, Nathan Jankowski, Harold L. Dibble, Paul Goldberg, Shannon P. McPherron, Dennis M. Sandgathe, and Marie Soressi

The age of three Middle Palaeolithic sites: single-grain optically stimulated luminescence chronologies for Pech de l'Azé I, II and IV in France

Zenobia Jacobs[1], *Nathan Jankowski*[1], *Harold L. Dibble*[2,3,4], *Paul Goldberg*[1,5], *Shannon P. McPherron*[4], *Dennis Sandgathe*[6], *Marie Soressi*[4,7]

[1]*Centre for Archaeological Science, School of Earth and Environmental Sciences, University of Wollongong, Wollongong, NSW, Australia 2522*

[2] *Department of Anthropology, University of Pennsylvania, Philadelphia, USA.*

[3] *Institute for Human Origins, Arizona State University, USA.*

[4] *Department of Human Evolution, Max Planck Institute for Evolutionary Anthropology, Leipzig, Germany.*

[5] *Department of Archaeology, Boston University, Boston, USA.*

[6] *Human Evolution Studies Program and Department of Archaeology, Simon Fraser University, Burnaby, Canada.*

[7] *Faculty of Archaeology, Leiden University, PO Box 9514, 2300 RA Leiden, The Netherlands*

Abstract

Optically stimulated luminescence (OSL) measurements were made on individual, sand-sized grains of quartz from Middle Palaeolithic deposits at three sites (Pech de l'Azé I, II and IV) located close to one another in the Dordogne region of southwest France. We were able to calculate OSL ages for 69 samples collected from these three sites. These ages reveal periods of occupation between about 180 and 50 thousand years ago. Our single-grain OSL chronologies largely support previous age estimates obtained by thermoluminescence dating of burnt flints at Pech IV, electron spin resonance dating of tooth enamel at Pech I, II and IV and radiocarbon dating of bone at Pech I and IV, but provide a more complete picture due to the ubiquitous presence of sand-sized quartz grains used in OSL dating. These complete chronologies for the three sites have allowed us to compare the single-grain ages for similar lithic assemblages among the three sites, to test the correlations among them previously proposed by Bordes in the 1970s, and to construct our own correlative chronological framework for the three sites. This shows that similar lithic assemblages occur at around the same time, and that where a lithic assemblage is unique to one or found at two of the Pech sites, there are no deposits of chronologically equivalent age at the other Pech site(s). We interpret this to mean that, at least for these Pech de l'Azé sites, the Mousterian variants show temporal ordering. Whether or not this conclusion applies to the wider region and beyond, the hypothesis that Mousterian industrial variation is temporally ordered cannot be refuted at this time.

KEYWORDS: optical dating; Typical Mousterian; Mousterian of the Acheulian Tradition; Quina Mousterian; Neanderthal

Introduction

As one of the sites presented in the seminal work of Lartet and Christy (1864) in the mid-19th Century, Pech de l'Azé I has earned its place in the development of the field of Palaeolithic archaeology. Around 150 years have now elapsed since that publication, and during this time many other sites in and around the Dordogne valley have been excavated, including three other Lower and Middle Palaeolithic locales in the immediate area of Pech de l'Azé I (Pech de l'Azé II-IV; Bordes, 1971; Soressi et al., 2007; Turq et al., 2011). Together, the Pech sites contain examples of most of the classic Mousterian "facies", or industrial variants as defined by Bordes (1960) and others (Peyrony, 1925), and thus continue to play a vital role in debates concerning the nature and interpretation of Mousterian assemblage variability (e.g., Mellars, 1965; Binford, 1973; Bordes, 1977; Rolland and Dibble, 1990; Delagnes and Rendu, 2011; Discamps et al., 2011). With the advent of new dating techniques over the past several decades, numerical ages have been obtained from a large number of sites in southwest France, including the Pech sites, by a variety of methods (e.g., Vogel and Waterbolk, 1967; Bowman and Sieveking, 1983; Valladas et al., 1986, 1987, 1999, 2003; Mellars and Grün, 1991; Falguères et al., 1997; Guibert et al., 1997, 1999, 2008; Lahaye, 2005; Guerin et al., 2012). Given the time-depth represented by the Pech archaeological deposits, which together are comparable to those of the classic, but still undated, reference site of Combe Grenal, and the size and variety of the archaeological assemblages, which together are far larger than those of Combe Grenal (Bordes' Pech IV collection exceeded his Combe Grenal collection [McPherron et al., 2012a]), it is not surprising that some of the earliest numerical ages for the French Mousterian have been obtained at these sites (e.g., Schwarcz and Blackwell, 1983; Grün et al., 1991) or that these sequences are a continuing focus of attention for both archaeologists and geochronologists (e.g., McPherron and Dibble, 2000; McPherron et al., 2001, 2012b; Dibble et al., 2005, 2009; ; Soressi et al., 2007, 2013; Texier 2009; Turq et al., 2011; Richter et al., 2013).

Prior to the present study, a number of dating studies were undertaken at the Pech sites, including electron spin resonance (ESR) dating of tooth enamel on teeth collected from Pech I, II and IV (Grün et al., 1991, 1999; Soressi et al., 2007; Turq et al., 2011), thermoluminescence (TL) dating of burnt flint from Pech IV (Bowman et al., 1982; Richter et al., 2013), radiocarbon (^{14}C) dating of charcoal and bone from Pech I and IV (Soressi et al., 2007; McPherron et al., 2012b) and uranium-series dating of flowstones in the cave connecting Pech I and II and in deposits at Pech II (Schwarcz and Blackwell, 1983). Only three optically stimulated luminescence (OSL) ages have been reported for the Pech sites and that was for one level at Pech I in Soressi et al. (2013) as part of the study fully presented here. At Pech I and II a single technique (ESR dating of tooth enamel) has been used to date the entire sequence. At Pech IV, no single technique was applied to the entire sequence; instead, different techniques have been used to date different portions of the deposit, with only a small amount of overlap. This is because animal teeth (for ESR dating) are not present in abundance in every layer, burnt flints (for TL dating) are available only in those layers where burning is evident, flowstones are rarely preserved in archaeological sections and may be too dirty for uranium-series dating, and most of the deposit is beyond the range of radiocarbon (^{14}C) dating.

In this study, we applied a single dating method to the sedimentary deposits at each of the Pech sites to provide a coherent chronology on a common time scale. We used single-grain OSL dating of quartz because quartz is ubiquitous in geological and archaeological deposits and has an OSL time range that can extend from a few years to a few hundreds of millennia. Because OSL dating

can be applied to geological and archaeological sediments, it was also feasible to obtain a complete chronological sequence for these sites – even for those layers that do not contain any archaeological traces. By applying single-grain OSL dating to each and every layer, it is thus possible to discern the history of site formation at a temporal resolution that might allow periods of occupation to be distinguished from periods of site abandonment.

There is also an archaeological imperative to link these sites using a common chronological yardstick. The three Pech sites have lithic assemblages that vary significantly within each site (Pech II and IV), that show some similarities between sites (e.g., Pech I and the top of Pech IV), and that occur at only one of the sites (e.g., small flake production in the so-called Asinipodian at Pech IV, Bordes 1975). The question thus arises: does the assemblage variability both within and between the Pech sites represent different/similar periods in time or is it because the caves were used for different/similar purposes at the same time? This basic question concerning Mousterian variability remains unresolved with, on the one hand, some stratigraphic and palaeoenvironmental data suggesting that the Mousterian variants represent chronological phases (Mellars 1970, 1989, 1992; Jaubert, 2012; Discamps 2013) while on the other an increasingly large set of numerical ages have failed to support a chronological succession (e.g., Valladas et al., 1999; Guibert et al., 2008; Vieillevigne et al., 2008; Richter et al., 2013). Although many numerical ages have been obtained for the Pech sites over the past few decades, the differing precisions and possible systematic biases in age determinations make it difficult to correlate the deposits with sufficient resolution based on previous dating evidence alone. A coherent and consistent chronology is required, therefore, to reliably compare the timing of the different artefact assemblages at each of the Pech sites and to overcome any distortion inevitably introduced by different dating methods.

Our goal in this paper is to develop an OSL chronology for the three Pech sites that will reveal when the lithic sequences for the three sites are broadly contemporaneous and when they are not. The three sites are located very closely within the same collapsed cave setting, where the same raw materials were also used for tool manufacture. This may increase the probability of similar behaviors being recorded at similar times. Though three sites are not enough to demonstrate that Mousterian variability is chronologically structured, they can falsify the hypothesis. If similar Pech industries are not broadly contemporary or if, in a given time slot, there is significant lithic variability, it suggests that the chronological phase argument for Mousterian variability cannot be supported. In doing this study, we will also test previous correlations of the sites, made by Bordes (1975) on the basis of faunal and sedimentological evidence, linked to the Riss-Würm climatic phase scheme.

Site background and stratigraphy

The hill of Pech de l'Azé contains a complex of four separate late Middle Palaeolithic collapsed cave sites (Fig. 1c), located in the department of the Dordogne in southwest France, situated about 5 km southeast of the city of Sarlat (44°50'N, 1°14'E) (Fig. 1a,b). The sites are positioned at the base of an Upper Cretaceous, Coniacian limestone cliff face (Goldberg et al., 2012), ~50 m above the valley floor of the Enéa River, a small tributary of the Dordogne River (Fig. 1c). Pech I and II are on either side of a still existing karstic tunnel, and Pech IV is thought to be part of the same karst system, though not the same karstic tunnel (Turq et al., 2011) (note that Pech III is a

small cave not far to the west of Pech II that is now empty of sediment). All three sites had a complex morphological evolution, including periods of cliff retreat and intense roof collapse that significantly changed their configuration over time (Texier, 2009; Turq et al., 2011). Understanding the sedimentology and the site formation processes at each of these sites is important for OSL dating, as this directly impacts on what we are dating – the last time sedimentary grains of quartz were exposed to sunlight. The sedimentology and site formation of all three sites have been documented thoroughly in Bordes (1972), Laville (1973), Goldberg (1979), Texier (2009), Turq et al. (2011) and Soressi et al. (2013). A summary of the stratigraphy, associated archaeological industries and the main sedimentological features of each layer and for each site are provided in Tables 1a, 1b and 1c.

Pech I

Pech I was originally excavated in the early 19th century by Jouannet and later by the Abbé Audierne, followed by excavations in 1909 by Capitan and Peyrony, in 1929-30 by Vaufrey and from 1948 to 1951, and again from 1970 to 1971 by Bordes. In 2004 and 2005 limited excavations were conducted by Soressi on the witness section left by Vaufrey in 1930, which has been used as the reference sequence for the site since then. A schematic of the site, location of each of the excavations and the witness section are provided in Fig. 2a.

The stratigraphy of Pech I consists of seven levels (Table 1a; Bordes, 1954-1955; Texier, 2009). Levels 3–7 are all attributed to the Mousterian of the Acheulian Tradition (MTA). Peyrony used Pech I as one of the type sites to define the MTA (Peyrony, 1925) and two variants of the MTA were later described, namely MTA Type A and MTA Type B (Bordes and Bourgon, 1951). The MTA Type A is characterized by the production and use of mainly bifaces, whereas the MTA Type B is characterized by fewer bifaces and by the production and use of backed knives and elongated flakes (Soressi, 2004). Layers 4–7 are of interest in this study and, in general terms, consist of a ~4 m thick deposit composed of very coarse blocks of collapsed limestone rubble embedded in a clayey sand matrix (Fig. 2b,c). The sediment is mostly derived from the slopes and was deposited as slope-wash, together with continuous large cliff and roof collapse (Texier, 2009).

The archaeological assemblage in Layer 4 is attributed to the MTA Type A; during the 2004 excavation by Soressi, a juvenile Neandertal tooth was found confirming that the MTA Type A was made by Neandertals (Soressi et al., 2007). The recent excavations also yielded a lissoir, a bone tool type likely used on hides, previously thought to have been made only by modern humans and, thus, adding to the knowledge of the complexities of late Neandertal behavior (Soressi et al., 2013). Several hundreds of blocks of black pigment, manganese dioxide, some of them bearing traces of use, have also been discovered in Layer 4 (Soressi and d'Errico, 2007; Soressi et al., 2008). Layer 5 has a low density of artefacts of both MTA Types A and B. Layers 6 and 7 are both attributed to MTA Type B; the very top of Layer 7 (the top ~1 m of the section), is archaeologically sterile (Fig. 2c). During the 1909 excavations by Capitan and Peyrony, a juvenile Neandertal skull and mandible were uncovered in Layer 6 (Fig. 2a; Soressi et al., 2007), confirming that the MTA Type B was also made by Neandertals.

Pech II

Pech II was excavated by Bordes between 1950 and 1969 (Bordes and Bourgon, 1950, 1951; Bordes 1969, 1971, 1972; Laville et al., 1980). It contains a total of 5 m of sediment and karstic and associated rock weathering deposits, formed at the entrance of a small cave that penetrates a small tunnel at the opposite end leading to Pech I (Fig. 1b and Fig. 3a). The Pech II sequence has previously been studied in detail, including aspects of sedimentology (Laville 1975; Goldberg, 1979; Laville et al., 1980; Texier, 2009), palynology (Paquereau, 1969), fauna (Bordes and Prat, 1965; Laquay, 1981), and the associated archaeological assemblages (Bordes and Bourgon, 1951; Bordes, 1971, 1975; Laville et al., 1980), but no recent excavations have taken place. A plan map of the site is shown in Fig. 3a together with a schematic of one of the sections that best represents the entire sequence (Fig. 3d).

The stratigraphy of Pech II was described by Bordes (1972) and Laville (1973) as 10 sedimentary layers, with many of the layers also divided into sub-layers; these are summarised in Table 1b and shown in Fig. 3d. Texier (2009) later re-defined the stratigraphy based on his sedimentological observations, and his layer assignations are also provided in Table 1b and Fig. 3d. We chose to use the stratigraphic layers of Bordes (1972) because we used Laville's stratigraphic drawing provided in Goldberg (1979) to select our sample locations in order to match the layers with the archaeological industries as closely as possible. The sedimentary and archaeological sequences can be divided into two broad phases, those below and those above the large cryoclastic deposit in Layer 5 (Fig. 3d). The deposits below were originally attributed to the Clactonian (Layers 6-8) and Acheulean (Layer 9) archaeological industries, whereas the deposits above comprise a range of different Mousterian industries, including Typical (Layers 3, 4A, 4C and 4D), Denticulate (Layer 4B) and Ferrassie Mousterian (Layer 2A-G).

Pech IV

Pech IV was discovered in 1952 by Bordes, but the first major systematic excavation was not undertaken by him until 1970, and he continued work there for a total of eight years. The Pech IV stratigraphy was first described in a preliminary note by Bordes in 1975. Further investigations of the Bordes collection by McPherron and Dibble (2000) and a new field campaign directed by them from 2000-2003, led to a re-investigation of the site formation processes, sedimentology and stratigraphy. A detailed description of the new stratigraphic framework, and the methods used, are reported in Turq et al. (2011).

The stratigraphy and basic sedimentological features of each of the layers are summarized in Table 1c. A planform map of the site is shown in Fig. 4a together with a schematic representation of the stratigraphy for the west wall (Fig. 4b). The archaeological assemblage comprises a range of different Mousterian industries, including Typical Mousterian (Layers 8, 5, 4C and 4B), the Asinipodian (Layer 6), the Quina Mousterian (Layer 4A) and the MTA (Layer 3). At the time of deposition of the basal Layer 8, the site was a cave rather than a rock shelter (Goldberg et al., 2012), and this layer represents a period of intense anthropogenic activity. The layer is distinctly different from all the other layers in that it consists of numerous hearth features that together give the layer a black and burnt appearance (Dibble et al., 2009; Goldberg et al., 2012). The first major collapse of the cave roof occurred on top of Layer 7, marked by the presence of a layer of limestone slabs that created a physical and chemical barrier, preserving Layers 7 and 8. This collapse resulted in a more

open configuration of the site. A significant break in sedimentation is found between Layers 6 and 5 in the form of a sharp and irregular contact. The culmination of the collapse of the cave ceiling over the cave mouth occurred at the end of Layer 5 and beginning of Layer 4, resulting in a further enlargement of the cave aperture. The previously poorly-illuminated and sheltered cave is now thought to have become open to the elements and is more akin to a rock shelter (Turq et al., 2011). A sharp erosional contact separates Layer 4 from Layer 3; cryoturbation is believed to have been the process responsible for the truncation of Layer 4A. Layer 3 is the last of the layers to contain in situ archaeological materials and is overlain by Layer 2, which is present only along the western section. After deposition of Layer 2, a complete collapse of the cave awning occurred and effectively sealed and preserved the site and archaeological sequence. Layer 1 was formed much later in historical time and is the result of colluvial processes, migrating slowly downhill, mantling the collapsed roof deposit of the site.

Age determination by OSL dating

OSL dating is the 'workhorse' in this study because it is able to generate accurate and precise ages over the timespan of interest and provides a means of determining burial ages for sediments and associated artefacts (Huntley et al., 1985; Aitken, 1998; Duller, 2004; Lian and Roberts, 2006; Jacobs and Roberts, 2007; Wintle, 2008; Guérin et al., 2015; Roberts et al., 2015). The method is based on the time-dependent increase in the number of trapped electrons induced in mineral grains (such as quartz) by low levels of ionising radiation from the decay of natural uranium, thorium and potassium in the surrounding deposits and from cosmic rays. The time elapsed since the light-sensitive electron traps were emptied can be determined from measurements of the OSL signal – from which the 'equivalent dose' (D_e) is estimated – together with determinations of the radioactivity of the sample and the material surrounding it to a distance of ~30 cm (the 'dose rate'). The OSL 'clock' is reset by just a few seconds of exposure to sunlight. The D_e divided by the dose rate gives the burial time of the grains in calendar years before present, enabling a direct comparison with other numerical age estimates (including calibrated ^{14}C ages and TL, ESR and uranium-series ages). Tests on known-age samples have shown that accurate OSL ages can be obtained from a wide variety of depositional environments (Rittenour, 2008) — including cave and rockshelter sediments, which are the focus of this study — provided that appropriate OSL signals are measured and rigorous procedural checks are made.

Material and methods

Sampling for OSL dating

Seventy-three samples were collected for OSL dating from the three sites. Both archaeological and non-archaeological layers were sampled, the latter to provide additional chronological and contextual information. All samples were collected in a manner that prevents inadvertent exposure of the sediment to sunlight that would reset the luminescence 'clock'.

We collected 20 OSL samples from Pech I at night using a red light for illumination. All OSL samples from the witness section (PdLI-7-20; Fig. 2b,c) were excavated using a trowel and/or auger. The samples collected from the cave wall (PdLI-1-6; Fig. 2d), above the Capitan and Peyrony/Bordes excavations (Fig. 2a), were stabilised with plaster bandages, and then cut out with a knife. The

location of each of the OSL samples is shown in Fig. 2c, and their positions were also recorded by total station relative to the site datum.

We collected 19 samples from Pech II, all during the day. The locations of the samples are shown in Fig. 3. All samples were collected as blocks of sediments that were stabilised with plaster bandages and cut out using a knife (shown as red boxes in Fig. 3 where the broken white line indicates the border between samples taken in a continuous column).

We also collected 30 samples from Pech IV, all at night, using a red light. The location of the two squares (C12 and G15) from which the samples were collected is shown in Fig. 4a as red squares, and the location of each of the samples is shown in Figs. 4c and 4d. We did not collect a sample from Layer 7, and the samples from Layer 8 are not part of the same continuous column of samples collected from the north face of square C12; instead, we collected the Layer 8 samples from the thickest extent of this layer further to the south into the west face of square G14 (Fig. 4d). The section faces were cleaned prior to sample collection to remove light-exposed grains. All samples were excavated using a trowel and placed into a plastic bag. Three samples (PdAIV-1, 2 and 3) were collected as blocks of sediment that were stabilised with plaster bandages and cut out using a knife (shown as red squares in Fig. 4c and 4d). One of these samples (PdAIV-1) was further sub-sampled into four samples (PdAIV-1A to 1D). All sample positions were recorded by total station relative to the site datum. Both types of samples were sealed in black plastic bags to prevent light exposure during transport to the laboratory.

In the OSL dating laboratory at the University of Wollongong, the sample bags were opened under dim red light. Where samples were collected as intact sediment blocks, these samples were kept as undisturbed sediment blocks and sub-sampled in the laboratory for OSL measurement. The remainder of the blocks was impregnated with resin and thin sections were made for further study of the sediments. Quartz grains were then extracted from the OSL samples using standard preparation procedures (Wintle, 1997; Aitken, 1998). First, carbonates were dissolved in 10% hydrochloric acid and then organic matter was oxidised in 30% hydrogen peroxide solution. The remaining sample was dried and then sieved to isolate grains of 180–212 μm in diameter, and feldspar, quartz and heavy minerals were separated by density using sodium polytungstate solutions of 2.62 and 2.70 specific gravities, respectively. The separated quartz grains were etched with 48% hydrofluoric acid for 40 min to remove the alpha-irradiated rind of each quartz grain and to destroy any remaining feldspars, and then rinsed in hydrochloric acid to remove any precipitated fluorides, dried and sieved again; grains retained on the 180 μm diameter mesh were used for dating.

Equivalent dose (D_e) determination

D_e values were estimated for individual 180-212 μm in diameter sand-sized grains for all but three (PdLI-6, PdLII-1 and PdLII-3) of the samples from all three sites. We used the standard Risø single grain aluminum discs (Bøtter-Jensen et al., 2000) for measurement of all individual grains, and confirmed the presence of only one grain in each hole after measurement by systematically checking each disc under a microscope.

All measurements were made in an identical manner and with the same equipment, using the single aliquot regenerative-dose (SAR) procedure described elsewhere (e.g., Murray and Wintle,

2000; Jacobs et al., 2008). The SAR procedure involves measuring the OSL signals from the natural (burial) dose and from a series of regenerative doses (given in the laboratory by means of a calibrated $^{90}Sr/^{90}Y$ beta source), each of which was preheated at 180°C for 10 s prior to optical stimulation by an intense, green (532 nm) laser beam for 2 s at 125°C. The resulting ultraviolet OSL emissions were detected by an Electron Tubes Ltd 9235QA photomultiplier tube fitted with Hoya U-340 filters. A fixed test dose (~10 Gy, preheated at 180°C for 5 s) was given after each natural and regenerative dose, and the induced OSL signals were used to correct for any sensitivity changes during the SAR sequence. A duplicate regenerative dose was included in the procedure, to check on the adequacy of this sensitivity correction, and a 'zero dose' measurement was made to monitor the extent of any 'recuperation' induced by the 180°C preheat. As a check on possible contamination of the etched quartz grains by feldspar inclusions, we also applied the OSL IR depletion-ratio test (Duller, 2003) to each grain at the end of the SAR sequence, using an infrared exposure of 40 s at 50°C.

The D_e values were estimated from the first 0.22 s of OSL decay, with the mean count recorded over the last 0.3 s being subtracted as background. The dose-response data were fitted using a saturating exponential function with an extra linear term, and the sensitivity-corrected natural OSL signal was projected on to the fitted dose-response curve to obtain the D_e by interpolation (see Supplementary Online Material (SOM) for example decay curves and dose response curves). The uncertainty on the D_e estimate of each grain (from photon counting statistics, curve fitting uncertainties, and an allowance of 2% per OSL measurement for instrument irreproducibility) was determined by Monte Carlo simulation, using the procedures described by Duller (2007). The final age uncertainty also includes a further 2% (added in quadrature) to allow for any bias in the beta source calibration; this error is added as a systematic uncertainty. The $^{90}Sr/^{90}Y$ beta source was calibrated using a range of known gamma-irradiated quartz standards for individual grain positions. Spatial variations in beta dose rate for individual grain positions were taken into account, based on measurements made using the same gamma-irradiated quartz standards (e.g., Ballarini et al., 2006). A relative error of 2.8% was added, in quadrature, to the combined random error of the D_e of each grain to capture the uncertainty associated with the calibration of the individual grain positions for the machine used in this study. The calibration of each grain position is based on multiple estimates of D_e from different grains that received a gamma dose that are then combined to obtain one value using the central age model of Galbraith et al. (1999). It is the relative error associated with the combined D_e value that is added as a random error to the D_e of each grain. Details of the dose recovery and preheat plateau tests to determine the preheat conditions for measurement of the grains are provided in the SOM (Table S1 and Fig. S1).

Of all the individual grains measured from all three sites (Pech I - n = 21,900; Pech II – n = 32,900; Pech IV – n = 56,900), only a very small number of grains (n = 1270, 1973 and 2403, respectively) were used for final D_e determination. Aberrant grains were rejected using the quality-assurance criteria described and tested previously (Jacobs et al., 2006). Supplementary Online Material Tables S2, S3 and S4 provide the details for all samples from all three sites and the reasons for why single grains were rejected. A discussion and examples of why grains have been rejected are provided in the SOM.

The majority of grains (on average ~90%) were rejected because they were too dim following a laboratory dose (T_N signal<3xBG) or the test dose signal was imprecisely known (>20%

error on test dose signal). From the ~10% grains that gave a measureable luminescence signal, ~20-30% of the grains were routinely rejected because they were sensitive to infrared radiation, failed the OSL-IR depletion ratio of Duller (2003) and gave D_e values that were half that obtained from quartz grains that behaved in an expected manner (see Fig. S5 and S6). Further discussion is provided in the SOM.

Decay curve and dose response curves for a number of grains from a representative samples from each site are provided in SOM Fig. S7 and S8, and the D_e values for all accepted grains are displayed as radial plots in SOM Fig. S9 (Pech I), Fig. S10 (Pech II) and Fig. S11 (Pech IV) for each of the samples. One representative example from each site is also shown in Fig. 5a-c. All the single grain D_e distributions are spread more widely than can be explained by measurement uncertainties alone. The single-grain D_e distributions are overdispersed by between 16 ± 2 (PdLI-20) and 53 ± 7% (PdLI-10) for samples from Pech I (Table 2), between 25 ± 3 (PdLII-6) and 40 ± 4% (PdLII-14) for samples from Pech II (Table 3), and between 17 ± 5 (PdLIV-13) and 38 ± 4% (PdLIV-8 and PdLIV-24) for samples from Pech IV (Table 4). The overdispersion values for the samples collected as block samples from Pech IV range between 38 ± 3 (PdAIV-1-D) and 72 ± 6% (PdAIV-1-B). There is no discrete patterning observed in any of the distributions that allows us to resolve post-depositional mixing or partial bleaching; all distributions are scattered randomly around a central value of D_e (SOM Figs. S9–11). We interpret the spread to be predominantly the result of differences in the intrinsic behavior of the grains, heterogeneity in the beta-dose delivered to individual grains of quartz and also small-scale disturbances by soil fauna and flora in some of the samples that may mix stratigraphically adjacent sediment through burrowing and root penetration. Investigation of thin sections of stratigraphically equivalent samples for Pech IV, and from the same sample positions for sample PdLI-1 to -6 and all the PdLII samples, support the possible effects from the latter two factors.

Since we cannot resolve any discrete and large-scale post-depositional mixing in any of our samples, we used the central age model (CAM) of Galbraith et al. (1999) to combine the single-grain D_e values meaningfully for all samples in order to obtain the most accurate estimate of D_e for age calculation. The CAM model assumes that the D_e values for all grains are centerd on some average value of D_e (similar to the median) and the estimated standard error takes account of any overdispersion (i.e., the greater the overdispersion, the larger the error; Galbraith et al., 1999). Information about the number of grains measured and used, overdispersion values calculated and the final $D_e \pm 1\sigma$ value for each sample are presented in Tables 2, 3 and 4 for Pech I, Pech II and Pech IV, respectively.

Dose rate determination

The total dose rate consists of contributions from beta, gamma and cosmic radiation external to the grains, plus a small alpha dose rate due to the radioactive decay of U and Th inclusions inside sand-sized grains of quartz. To calculate the OSL ages, we assumed that the measured radionuclide activities and dose rates prevailed throughout the period of sample burial. An internal alpha dose rate of 0.032 ± 0.01 Gy/ka (kilo-annum) has been assumed for all samples. We estimated the beta dose rates directly by low-level beta counting of dried, homogenised and powdered sediment samples in the laboratory, using a GM-25-5 multi-counter system (Bøtter-

Jensen and Mejdahl, 1988). We prepared and measured samples, analyzed the resulting data and calculated beta dose rates and errors following the procedures described and tested in Jacobs and Roberts (2015). GM-25-5 beta counting is the method of choice because this method is less sensitive to potential inaccuracies arising from U disequilibrium. Numerical modelling has shown that even the most common time-dependent disequilibria in the ^{238}U series are unlikely to give rise to errors in the total dose rate of more than 2–3% when emission-counting techniques such as GM-25-5 beta counting are employed (Olley et al., 1996, 1997). For all samples, allowance was made for the effect of sample moisture content (Aitken, 1985), grain size (Mejdahl, 1979) and hydrofluoric acid etching (Bell and Zimmerman, 1978) on beta-dose attenuation.

To test the accuracy of our beta dose rate estimates obtained from GM-25-5 beta counting, we also determined the beta dose rates in two additional ways. For the majority of samples from all three sites, we obtained estimates of U and Th from ICP-MS and K from ICP-OES to calculate the first additional set of beta dose rates. For all samples from Pech I and Pech II, we also obtained estimates of U and Th from thick source alpha counting (TSAC) and K from X-ray fluorescence (XRF) to determine the second additional set of beta dose rates. All elemental concentrations were converted to dose rates using the conversion factors of Guérin et al. (2011). We do not expect perfect agreement between the three different methods, since ICP-MS only measures the parent radionuclide in the U and Th decay series. GM-25-5 beta counting and combined TSAC and XRF measurements provide data on present-day dose rates from the full U and Th decay chains and from K. Since more than 60% of the beta dose rate from U is derived from the daughter nuclides lower down the decay series (e.g., post-^{226}Ra) and as disequilibrium in the U decay series is commonplace in limestone environments, estimates of U from ICP-MS can result in inaccurate estimates of the beta dose rate from the entire U chain. Comparisons of the estimates derived using the different methods will, therefore, also provide an idea of the relative extent of disequilibrium.

Gamma dose rates were measured directly at the vast majority of sample locations by in situ gamma spectrometry, to take into account any spatial heterogeneity in the gamma radiation field within 30 cm of each OSL sample (as gamma rays can penetrate this distance through sediment and rock). Counts were collected for 60 min with either a 1-inch (Pech II and Pech IV) or a 2-inch (Pech I) NaI (Tl) crystal. We measured the gamma dose rate of the limestone wall from which we collected the samples in Pech I and used this as an estimate of the gamma dose rate for half of the gamma sphere; we calculated the gamma dose rate for the other half of the gamma sphere from laboratory measurements of the sediment and combined those two estimates. The detectors were calibrated using the concrete blocks at Oxford University (Rhodes and Schwenninger, 2007) and the gamma dose rates were determined using the 'threshold' technique (Mercier and Falguères, 2007). This approach gives an estimate of the combined dose rate from gamma-ray emitters in the U and Th chains and from ^{40}K.

Account was also taken of the cosmic-ray contribution, which was adjusted for the average site altitude (~165 m), geomagnetic latitude (47.3°), density and thickness of rock and sediment overburden (Prescott and Hutton, 1994), and the $\cos^2$-Φ zenith angle dependence of cosmic rays (Smith et al., 1997). We also took into account the morphological evolution of the sites (see Texier, 2009 and Turq et al., 2011). The beta, gamma and cosmic-ray dose rates were corrected for long-term water contents. We used the current measured field values, which ranged between 0.5 and 7.4% at Pech I (Table 2), between 0.7 and 8.3% at Pech II (Table 3) and between 2.5 and 9.3% at Pech

IV (Table 4). A relative uncertainty of ±25% (at 1σ) was assigned to each estimate of water content. In general, the calculated total dose rate will decrease, and the calculated OSL age will increase, by ~1% for each 1% increase in water content.

Pech I The dose rate results for all samples from Pech I are provided in Table 2. The total dose rates for all the samples show only a modest amount of variation, ranging between 0.82 ± 0.04 (PdLI-9) and 1.29 ± 0.07 Gy/ka (PdLI-18), with the majority of values ranging between 0.9 and 1.1 Gy/ka.

Many of the OSL sample positions at Pech I were determined by reference to the locations of previously made large holes for gamma spectrometry by W.J. Rink in 1999/2000. Not much sediment is left at Pech I, so to preserve as much of the remaining deposit as possible, and still make the required in situ gamma spectrometry measurements, we collected some of our samples inside and adjacent to Rink's gamma spectrometry holes, and made our own gamma spectrometry measurements inside these same holes. This allowed us to check the consistency of the gamma dose rate measurements conducted by two different laboratories more than a decade apart, and also gave us the estimate of the gamma dose rate at the point of sampling. We compared our estimates of the gamma dose rate with those of Jones (2001) and Soressi et al. (2007), which were obtained for the same holes. The results are shown in Fig. 6, from which it can be seen that there is good consistency between the measurements made by the different laboratories. On average, the gamma dose rate ratio of Rink / this study is 0.95 with a standard deviation of 0.05. What is interesting is the significant range in gamma dose rates of between ~0.23 ± 0.01 and 0.63 ± 0.03 Gy/ka, especially between the sediments near the top and bottom of the ~4 m-tall witness section, but also for sediments within the same layer. For example, two gamma dose rate measurements in Layer 4, taken ~50 cm apart, gave gamma dose rates of 0.63 ± 0.03 and 0.52 ± 0.03 Gy/ka, respectively, with another sample from Layer 4 giving a gamma dose rate of 0.36 ± 0.02 Gy/ka. This difference is directly related to the proximity of the samples to blocks of limestone. Such spatial variations may prove problematic when the gamma dose rate has to be reconstructed for stone artifact (TL dating) or tooth (ESR dating) samples that were obtained from museum collections and for which only a site-average estimate is used for age estimation. An advantage of OSL dating of sediment in settings where there are gross inhomogeneities in the gamma sphere of influence, is the determination of the gamma dose rate in the field at the point of sampling.

The beta dose rates determined in three different ways are shown as ratios in Fig. 7 for all samples from Pech I. From here it can be seen that the beta dose rates derived using elemental concentrations from ICP-MS are systematically smaller than those derived using the two alternative methods, which is likely the result of uranium leaching. Average ratios of 0.93 ± 0.03 and 0.92 ± 0.03 (one significant outlier was omitted from the latter ratio) were calculated for the ICP-MS beta dose rates divided by those obtained from GM-25-5 beta counting and a combination of TSAC and XRF, respectively. The latter two techniques show good consistency, resulting in an average beta dose rate ratio of 1.01 ± 0.03. The uncertainties reported above are the standard deviations of the average ratio.

Pech II The dose rate results for all samples from Pech II are provided in Table 3. The total dose rates for all the samples range between 1.09 ± 0.07 (PdLII-15) and 1.49 ± 0.08 Gy/ka (PdLII-17), with one lower value at 0.97 ± 0.05 Gy/ka (PdLII-12). Most values appear to fall into two groupings, centerd

on ~1.2 and ~1.45 Gy/ka. From studies of the thin sections made on the same samples, it appears that the difference relates directly to the relative proportion of clay and limestone in the sediment.

No in situ gamma spectrometry results have previously been reported for this site. The values reported in Grün et al. (1991) were based on measurements of parental concentrations of U and Th, and of K, in the sediment attached to the dated tooth samples, using neutron activation analysis (NAA). Neutron activation analysis does not take into account any possible disequilibrium that may exist in the U-series decay chain or spatial inhomogeneity in the gamma sphere (~30 cm radius), so it suffers from the same limitations as ICP-MS. We measured the in situ gamma dose rates for a number of our samples and these are indicated as filled circles in Fig. 3, with the results provided in Table 3.

The beta dose rates determined in three different ways are shown as ratios in Fig. 8 for all samples from Pech II. No systematic trends among any of the methods can be seen; rather, the beta dose rate ratios are spread randomly around a ratio of unity, with the occasional significant outlier, resulting in average beta dose rate ratios and standard deviations of 1.01 ± 0.13, 1.02 ± 0.15 and 0.99 ± 0.11 for the various combinations (Fig. 8).

Pech IV The dose rate results for all samples from Pech IV are provided in Table 4. The total dose rates range between 0.79 ± 0.05 (PdLIV-1) and 1.59 ± 0.08 Gy/ka (PdLIV-18). Richter et al. (2013) reported in situ gamma dose rate results based on measurements of α- Al_2O_3:C dosimeters with OSL. Their results are presented in Fig. 9 as closed circles, where each circle represents the result from one dosimeter. Also shown, as open triangles, are the in situ gamma spectrometry measurements made in this study. We measured the gamma dose rates for each of our samples, the locations of which are shown in Fig. 4 (except PDAIV-1-C and PDAIV-1-A). Note that the results from the two studies are not directly comparable, unlike for Pech I (Fig. 6), as the measurements at Pech IV were made on similar sediment from the same layers, but from different profiles within the cave (see Fig. 4, and Fig. 3 of Richter et al. [2013], for exact locations). The average gamma dose rate for each layer derived from each of the methods is shown inside the stippled boxes in Fig. 9, and the ratio of the two average values is provided above each of the boxes. The results from Layers 4C and 5A show good consistency. The two α- Al_2O_3:C dosimeter results for Layer 3B are quite different; all of the in situ gamma spectrometry results are consistent with the lower dose rate values measured for the other layers.

PdAIV-1 was collected as a block sample and sub-sampled into four samples (PdAIV-1A to 1D). We were able to use the in situ gamma spectrometer measurements for PDLIV-1 and PDLIV-2 as direct equivalents of PdAIV-1-D and PDAIV-1-B, respectively, but the gamma dose rates for the remaining two samples (PDAIV-1A and PDAIV-1-C) had to be calculated separately. PdAIV-1-C is located half way between sub-samples B (above) and D (below). The gamma dose rate for this sample was taken as the average of the gamma dose rates from these two bounding samples. The gamma dose rate for sub-sample A, at the top of the Layer 8 sediment block (PDAIV-1), was considered to have received half its gamma dose rate from the underlying sediments, with the other half derived from the overlying limestone slabs. The first half was calculated from the in situ measurement made for sub-sample B (0.33 ± 0.02 Gy/ka; Table 4). The other half was based on the gamma dose rate measured from a sub-sample of the limestone that was powdered. Using this powdered sample, a gamma dose rate of 0.15 ± 0.01 Gy/ka was determined using a combination of

GM-25-5 beta counting and thick-source alpha counting. Therefore, the gamma dose rate for sub-sample A was determined to be 0.24 ± 0.01 Gy/ka (Table 4).

The beta dose rates from Pech IV were determined using only two different methods, namely GM-25-5 beta counting and conversion of measured concentrations of U, Th (ICP-MS) and K (ICP-OES) to beta dose rates. The ratios of the beta dose rates derived using these two methods are presented in Fig. 10a. The results for Pech IV are quite different from those obtained for Pech I and II. The beta dose rate ratios for some layers (e.g., 4A and 4C) are consistent with unity, whereas the ratios for sediment from other layers (e.g., 3A, 4B and 6A) deviate significantly from unity. The same bow-shaped curve can also be seen when U concentrations (ppm) derived from ICP-MS measurements are plotted (Fig. 10b). We interpret this similarity in shape to mean that the difference in the two calculated beta dose rates relates directly to the state of disequilibrium in the U decay series. Assuming that this U disequilibrium has prevailed throughout the burial history of the sample, or occurred only recently, then an excess of parental U will result in an overestimation of the beta dose rate using ICP-MS relative to GM-25-5 beta counting and the opposite is true in the case of a parental U deficit. If this interpretation is correct, then the beta dose rates derived using GM-25-5 beta counting provide more accurate estimates of the beta radiation component of the total dose rate, as this method is less sensitive to potential inaccuracies arising from U disequilibrium.

Assessing self-consistency of stratigraphic units

We used the statistical (homogeneity) test of Galbraith (2003), and the resulting *p*-values to test whether the independent estimates obtained within each stratigraphic unit are self-consistent (i.e., the spread in ages are compatible with the size of the uncertainties). If self-consistency is demonstrated (i.e., p = >0.05), we then calculated a weighted mean age estimate for each layer or sub-layer. Both *p*-values and weighted mean ages were calculated by combining all ages using only their random uncertainties (the errors provided in brackets after the age in Tables 2, 3 and 4). The final error on the weighted mean, however, includes the systematic error that was added in quadrature to the random error on the mean age. In calculating a weighted mean age for each layer, we assume that the individual age estimates within a layer represent either a single event, or a series of events spread over a period of time that is short compared to the size of the age uncertainties.

Results and preliminary discussion

Ages and comparisons with existing chronologies at Pech de l'Azé

The final ages for all samples from all three sites are listed in Tables 2, 3 and 4, together with the supporting D_e and dose rate estimates. Uncertainties on the ages are given at 1σ (standard error on the mean) and were derived by combining, in quadrature, all known and estimated sources of random and systematic error. The 1σ error on the age provided in brackets includes only the random errors and is the error to be used for comparison of ages among the three sites. For all other comparisons the full error should be used. For the sample D_e, the random error was obtained from the CAM used to determine the weighted mean, and a systematic error (of 2%) was included for any possible bias associated with calibration of the laboratory beta source. The total uncertainty on each

dose rate was obtained as the quadratic sum of all random (measurement) errors and the systematic errors associated with estimation of the beta and cosmic-ray dose rates.

Pech I ages We were able to obtain reliable ages for all samples collected from Pech I, including those sediment remnants from the Capitan and Peyrony excavations that were left on the cave wall. Very little variation in age was obtained for the samples collected from Layers 4, 5, 6 and 7 from both the witness section and the cave wall. The individual ages are plotted in Fig. 11a (closed symbols represent samples from the witness section and open symbols those samples collected from the cave wall). The ages range between ~46 and 55 ka.

The *p*-values for each layer are provided in Table 2 and range between 0.61 and 0.99, far greater than the accepted alpha value of >0.05, thus supporting self-consistency of ages within each layer. Accordingly, we calculated weighted mean ages for each of the layers and obtained ages of 51.2 ± 2.4 ka (Layer 4), 53.2 ± 2.9 ka (Layer 5), 52.2 ± 3.1 ka (Layer 6) and 48.8 ± 2.8 ka (Layer 7). The weighted mean ages for each layer are provided in Table 2 and plotted in Fig. 11b. In Table 2, the weighted mean ages for those layers where samples were collected from both the witness section and the cave wall were calculated separately to check for age consistency over space; the results support the consistency. A grand weighted mean was then calculated to include both samples from the wall and the witness section for that particular layer; it is these grand weighted mean ages that are plotted in Fig. 11b. It is apparent from Fig. 11b that the weighted mean ages for all four layers are consistent at 1σ uncertainty and when all the ages are combined a *p*-value of 0.99 is obtained, suggesting that there is no statistical difference in age between the top and the bottom and that the deposits, therefore, represent a relatively short duration of time; a weighted mean age of 50.7 ± 2.5 ka is obtained when all 19 age estimates are combined and is indicated as a stippled line and gray shading in both Fig. 11a and 11b.

It can be seen from Fig. 11b that when the weighted mean ages are plotted for each of the layers, there is a slight tendency, albeit within statistical uncertainty, for the middle two layers (Layers 5 and 6) to be older than the lowest layer (Layer 4); this was also the case for the ESR ages presented in Soressi et al. (2007). To further investigate this, we also plotted the weighted mean ages for the same set of samples, but when the two alternative estimates of beta dose rate are used instead to calculate the age (see Fig. 7 and section on beta dose determination); the results are also plotted in Fig. 11b. This same tendency is observed for all three data sets with the most extreme tendency demonstrated for those ages for which the beta dose rates are based on measured elemental concentrations determined with ICP-MS (U and Th) and ICP-OES (K). This supports our interpretation of the beta dose rates in Fig. 7 (and discussed above) that at some point in the past there was leaching of U (no thin sections were collected to further document leaching effects), and that the best estimate beta dose rate, and, hence, best-estimate age for these samples, are those using the beta dose rate obtained from GM-25-5 beta counting (plotted as open circles). The data suggest that the age of the MTA Type B and A at Pech I span a relatively short period of time (~2-4 ka), and all the ages are statistically consistent with a mean age of 50.7 ± 2.5 ka.

Pech I comparisons with published chronologies A series of ESR ages and three ^{14}C ages were previously reported by Soressi et al. (2007) for Pech I. They reported the mean ESR age and standard

deviation for three layers (Layers 5, 6 and 7) using two different uranium uptake models, namely the early-uptake (EU) and linear-uptake (LU) models. Soressi et al. (2007) also reported coupled ESR/U-series ages for two of the samples, one each from Layers 6 and 7 and three ^{14}C ages on bone from Layers 4 and 6. These ages are plotted, together with the OSL ages of this study, in Fig. 12. The EU and LU ages are shown as closed and open triangles respectively, and are treated as a single age range with the most likely age being somewhere between those two estimates. The ^{14}C ages are plotted with their 2σ ranges where the symbol denotes the midpoint value and the positive and negative error bars the entire calibration range.

Mean EU and LU ages for Layer 5 of 49 ± 6 and 51 ± 7 ka, respectively, are entirely consistent with the weighted mean OSL age of 53 ± 3 ka. Mean EU and LU ages of 40 ± 2 and 47 ± 5 ka, respectively for Layer 6 and a single coupled ESR/U-series age of $43\frac{+8}{-6}$ ka for one of the two measured teeth gave ages that are systematically younger than the weighted mean OSL age of 52 ± 3 ka; the ages are, however, consistent within their margins of error. The mean EU and LU ages of 42 ± 8 and 49 ± 7 ka, respectively, and the single coupled ESR/U-series age of $51\frac{+7}{-9}$ for Layer 7 is consistent with the weighted mean OSL age of 49 ± 3 ka. It is important to point out that the uranium concentrations for the enamel from the teeth were very low and that the external beta, gamma and cosmic-ray dose rates (i.e., the same dose rates that apply to the OSL ages) were responsible for at least half of the total dose rates. This means that the ESR ages will suffer from the same dosimetry issues related to the OSL samples (discussed above and shown in Fig. 7); this is in addition to the problem of recreating a dose rate environment that does not exist anymore because the sediments in which the teeth were buried have already been excavated. These issues may account for the variability in age between individual teeth from the same layer and also the larger errors associated with the ESR ages. Regardless, the two independent chronologies show good consistency and it appears that the LU modelled ages are more consistent with the OSL than the EU ages (Fig. 12).

The two ^{14}C ages on unburnt bone from the top of Layer 6 ranged at 2σ between ~ 44 and 41 cal ka BP (thousands of calibrated years before present) and this is younger than both the ESR and OSL ages for this layer (Fig. 12); there is no statistical overlap between the ^{14}C and OSL ages even at 2σ. The ^{14}C age from Layer 4 ranges at 2σ between 47 and 44 cal ka BP and is similarly younger than the corresponding OSL ages. The bone samples were not prepared using molecular ultrafiltration, so the underestimation may be due to small-scale contamination, now known to be a prevalent problem (e.g., Higham, 2011).

Pech II ages The ages for 17 samples from Pech II are provided in Table 3. The ages range between ~55 and 100 ka for the 10 sediment samples located above the thick cryoclastic complex (Fig. 3), and then again between ~140 and 180 ka for the seven sediment samples located below the cryoclastic complex. The ages are also displayed in Fig. 13 as a function of layer.

We did not attempt to date the fluvial sands at the base of the deposit in Layer 10 because we do not believe that these sands were exposed to sunlight prior to deposition. Texier (2009) indicated that deposition of these sands were subterranean in the endokarstic system. We obtained a single age of 165 ± 16 ka for Layer 9 which has been attributed to an Acheulean with handaxes (PdLII-15). We also obtained a single age of 159 ± 11 ka for Layer 8 (PdLII-7). We calculated a

weighted mean age of 170 ± 8 ka for four samples from Layer 7B and the sample from Layer 7A gave an age of 143 ± 9 ka (PdLII-2). Layers 8, 7B and 7A have all been called Clactonian with choppers and chopping tools but no handaxes. The D_e values for all these samples are close to saturation, so it may be that these ages represent minimum ages for these samples. The range of dose response curves, some not close to saturation, and the reproducibility of the D_e values, regardless of the shape of the curves, together with the consistency of these OSL ages with the ESR ages, however, may suggest that these ages are not significantly underestimated. It, therefore, appears that the sediment below the cryoclastic deposit in Layer 5 was deposited during, or before, the penultimate glacial period (marine isotope stage (MIS) 6). Although we could not date Layer 5, the cryoclastic layer, it was likely a result of the severity of the end of MIS 6, after which temperatures increased rapidly by ~14°C from a mean palaeotemperature of ~7°C to a mean palaeotemperature of ~21°C at the beginning of MIS 5 in southwestern France (Wainer et al., 2011).

Immediately above the cryoclastic deposit, the first evidence for occupation occurred at the base of Layer 4 in Layer 4E and 4D. Bordes (1972) described these layers, and the associated archaeological assemblages, as being significantly damaged by cryoturbation. Our first samples were collected across Layers 4D and 4C2 for which micromorphological analysis of our sample (PdLII-19) shows only limited evidence for cryoturbation in the form of coatings and some banded fabrics. The deposits appear quite fresh and intact with perhaps some of the fine fraction removed by water. We obtained an OSL age of 105 ± 7 ka (PdLII-19) for initial re-occupation of the site, associated with a Typical Mousterian industry. Layer 4B is associated with a lithic assemblage that is quite different from the preceding Typical Mousterian and was assigned to the Denticulate Mousterian. We obtained ages of 80 ± 6 ka (PdLII-18) and 90 ± 6 ka (PdLII-17) for Layer 4B. There is a significant age gap separating the age for Layer 4B and that obtained for Layer 4A1. The samples were collected only cm apart in depth (Fig. 3d and e), thus suggesting that there was also a significant break in sedimentation, or an erosional event that removed sediment from the site. It is interesting to note that this break was not visible in the field. An age of 58 ± 4 ka (PdLII-16) was obtained for this layer, which albeit rather poor in lithics is associated with the Typical Mousterian, and an age of 61 ± 5 ka (PdLII-14) was obtained for the Typical Mousterian in the overlying much lithically-richer Layer 3. Five ages from Layer 2G, associated with a scraper-rich Mousterian, gave a weighted mean age estimate of 60.1 ± 2.9 ka. The rest of Layer 2 was not sampled and was almost devoid of tools. Importantly, no MTA industry was identified in Pech II.

Pech II comparisons with published chronologies A series of ESR ages and two U-series ages were previously reported by Grün et al. (1991) and Schwarcz and Blackwell (1983) for Pech II, respectively. Grün et al. (1991) reported ages for 27 individual teeth collected from all major stratigraphic units and for the majority of the teeth, sub-samples were also measured. The U-series ages were reported for one in situ flowstone at the top of Layer 3 and a broken off stalagmite found within the cryoclastic deposit in Layer 5. All the ages are shown together with the OSL ages of this study in Fig. 14a and b where Fig. 14a shows the ages above the cryoclastic deposit and Fig. 14b those within and below this layer. The ESR ages represent averages of the different individual fragments of each tooth that was measured.

The ESR ages above the cryoclastic deposit (Layer 5) range between ~40 and ~90 ka, and the majority of the samples show excellent agreement between the EU and LU modelled ages, but there appear to be some age reversals. The ages from within and below Layer 5 range between ~130 and

220 ka. These EU and LU modelled ages show less agreement, but Grün et al. (1991) made a case for the EU modelled ages to be the more accurate. This was later further investigated in Grün et al. (1999) where it was apparent that it is difficult to choose one or the other and that further studies are required to refine the chronology. In a general sense, the ESR ages are in broad agreement with the OSL ages reported in this study. Both methods suggest two major phases of occupation above and below the cryoclastic deposit. The OSL ages in Layers 2, 3 and 4, however, show improved stratigraphic consistency and also indicate a major hiatus within Layer 4 that was not resolved with the ESR ages.

Schwarcz and Blackwell (1983) also reported U-series ages for Pech II. They dated an in situ flowstone at the top of Layer 3 and reported an age of 103^{+30}_{-25} ka. This age is much older than the corresponding ESR and OSL ages, but the errors are large and it is, thus, broadly consistent. They also obtained an age of 240 ka on a broken stalagmite in Layer 5, but this stalagmite is not in primary position and can only be used as a maximum age for the deposit.

Pech IV ages We were able to obtain reliable ages for all 27 samples collected from Pech IV. We also obtained an additional six ages from three different block samples (denoted as PdAIV in Table 4) from Layers 4A, 5B and 8. The ages range from ~50 ka near the top of the sequence in Layer 3A to ~100 ka at the base of the sequence in Layer 8. The ages and their associated uncertainties are listed in stratigraphic order in Table 4, together with the *p*-values and weighted mean ages for each layer.

The individual ages are plotted in Fig. 15 as a function of depth from where it can be seen that the ages are all in good stratigraphic order. Figure 15b shows the weighted mean ages for each layer to which a two period moving average regression line was fitted. This line clearly indicates that the sedimentation rate was not constant over time (as would be expected), and that during periods of most intense occupation (e.g., Layer 8, 6, 5A and 3) the sediment accumulated rapidly compared to the much slower accumulation rate associated with Layer 4 in which evidence of occupation was also sparse.

We have demonstrated in Fig. 10a that the beta dose rate results, when measured in two different ways, show significant divergence from each other in some parts on the sediment profile possibly because of the mobility of uranium (Fig. 10b). We postulated that the beta dose rates derived using GM-25-5 beta counting is superior and this is further supported in Fig. 16a where the ages for all the samples from Pech IV are plotted twice, once using the beta dose rate derived from GM-25-5 beta counting (closed circles) and the other using the beta dose rate derived from ICP-MS measurements (open triangles); for clarity the associated errors are not shown in this figure, but they are included in the age ratios shown in Fig. 16b. Figure 16a clearly shows an increase in age with an increase in depth using GM-25-5 beta counting, compared to the occasional significant age reversals obtained using ICP-MS measurements, especially for samples from Levels 6A, 4B and 3A.

We are, therefore, confident in our ages presented in Table 4 that use GM-25-5 beta counting for estimation of the beta dose rate and in the weighted mean age estimates determined for each of the layers. A weighted mean age of 93.9 ± 4.4 ka (Layer 8) was obtained for the lowermost archaeological deposit that can be characterized as Typical Mousterian. We did not collect a sample from Layer 7, so its age remains unknown. An age of 76.7 ± 3.7 ka was obtained for Layer 6 that contains the so-called Asinipodian industry with its emphasis on small flakes and is

significantly younger than the underlying Layer 8. This time gap may be represented by the undated and cryoturbated Layer 7, or the site may have been abandoned before or after the initial collapse of the cave roof that covers these two layers. The age of 76.3 ± 4.0 ka for Layer 5 (Typical Mousterian) is almost identical to the age obtained for Layer 6 (Asinipodian) and does not support the macroscopic observation of a sharp and irregular contact between these two layers (Turq et al., 2011). A significant break in sedimentation was suggested (Turq et al., 2011), but it may be that the duration of this break is shorter than the uncertainties on our age estimates. Based on the ages alone, it appears to have, instead, been a period of rapid sedimentation (Fig. 15b). Chronologies, however, should never be interpreted in isolation from other proxies and information. With OSL, we estimate the last time the sedimentary grains were exposed to sunlight. If the sediment in Layer 5 was re-deposited from sediment inside the cave as a result of colluvial or solifluction re-working the sediment (as proposed in Turq et al., 2011), and was not re-exposed to sunlight, then this age may well be an overestimate of the age for this layer, but its minimum age can be constrained by the age of 68 ± 4 ka for the overlying Level 4C.

Layer 4 shows a continuum of ages from ~70 ka through to ~58 ka, and the sedimentation was relatively slow compared to periods before and after. It is also the layer with the sparsest archaeological evidence. Three sub-levels were identified based on differences in sedimentology. The weighted mean ages of 68.3 ± 3.9 ka (Level 4C), 61.5 ± 3.4 ka (Level 4B) and 57.3 ± 2.8 ka (Level 4A), best constrain the age of this layer. Levels 4C and 4B are representative of the Typical Mousterian, whereas Level 4A contains Quina Mousterian (Turq et al., 2011). So our best age estimate of the Quina Mousterian at Pech IV is 57.3 ± 2.8 ka. The final occupation in Pech IV – Layer 3 – has been attributed to the MTA, for which we obtain weighted mean ages of 51.0 ± 2.6 ka (Level 3B) and 51.1 ± 2.4 ka (Level 3A).

Pech IV comparisons with published chronologies Three other independent dating techniques have been employed at Pech IV — ^{14}C dating of bone, ESR dating of tooth enamel and TL dating of burnt flints. All three techniques were used to obtain ages for Layer 3, but only TL dating was used to date three of the other layers (Layers 4C, 5A and 8). All the OSL ages are plotted in Fig. 17 together with the ^{14}C, ESR and TL ages. The ages are plotted for each layer and also shown, as stippled lines, are the weighted mean ages and 1σ standard errors calculated for the OSL ages for each layer. All OSL ages are shown as filled circles, EU- and LU-modelled ages are shown as closed and open triangles, respectively, TL ages as open diamonds and ^{14}C ages as lines where the line denotes the mid-point value of the 2σ calibration range.

It can be seen for Layer 3 that both the EU and LU modelled ESR ages and the TL ages are statistically consistent with the OSL ages. The ^{14}C ages that can be calibrated are consistent with the other ages at 2σ (see red stippled lines in Fig. 17). Also, the weighted mean OSL age is only slightly older than the start age of 49.5 cal ka BP at the lower end of the 2σ range for Layer 3 calculated using a Bayesian model and presented in McPherron et al. (2013). There are also two ^{14}C age estimates for Layer 3B that fall beyond the capability of the currently accepted ^{14}C calibration curve (IntCal13; Reimer et al., 2013), and these are shown with an arrow pointing upwards to indicate that they are minimum ages. Both these ages must be >50 cal ka BP and are thus consistent with the other independent ages.

The TL and OSL ages for Layers 4C, 5A and 8 also show excellent agreement. Richter et al. (2013) reported two TL ages for Level 4C of 69 ± 7 ka and 72 ± 7 ka, and these agree with the weighted mean OSL age of 68 ± 4 ka. They also reported a weighted mean TL age (n = 4) for Level 5A of 74 ± 5 ka that is in agreement with the OSL weighted mean age of 76 ± 4 ka, and a weighted mean TL age for Layer 8 (n= 6) of 96 ± 5 ka that is consistent with the OSL weighted mean age of 94 ± 4 ka.

Discussion

Bordes (1975, 1978) used the information he gathered based on the archaeological industries, fauna and, in particular, the geological work of Laville (1973) to correlate the three sites and to place the archaeological deposits within a climatic framework using the Würm and Riss climatic phases that were in vogue in Europe at the time. His proposed correlations are presented in Table 5. Bordes placed all of Pech I in Würm II (similar to OIS 3), together with the uppermost layers of Pech IV (Layers F1-4). These layers were attributed to the MTA Type A and B industries. The rest of Pech IV and the deposits above the large cryoclastic deposit in Pech II were all placed in Würm I (roughly equivalent to later MIS 5). The deposits below the cryoclastic layer in Pech II were all placed within the Riss (similar to MIS 6). Bordes drew direct parallels between only a few layers, including the MTA layers in both Pech I and Pech IV, in particular Layer 4 at Pech I and F4 at Pech IV (MTA-A) and Layers 6 and 7 at Pech I and F1 and F2 at Pech IV (MTA-B), as well as Layer 4C at Pech II and Layer X at Pech IV (Typical Mousterian). He recognized the lithics to be typologically similar and suggested they belong to the same climatic and chronological phases. He also recognized that some assemblages had no equivalents among the three different sites, and saw these as assemblages made by different groups of people occupying the sites during the same climatic phase, but perhaps centuries earlier or later. Bordes, thus, interpreted the deposits to span a relatively short, and almost continuous, period of time and suggested that the temporal control so far achieved is not fine enough, and that it probably will never be (Bordes, 1978). These correlations have since drawn substantial criticism (Mellars, 1988; Bertran and Texier, 1995; Texier, 2000).

The common chronology for all three Pech sites presented here now enables us to test the correlations proposed by Bordes (1975, 1978). In this study, we made measurements on individual sand-sized grains of quartz to maximize the benefits inherent in single-grain OSL dating. These include the identification of contaminant grains in a sample and their exclusion before final age determination, and the ability to directly check the stratigraphic integrity of archaeological sequences and take into account any post-depositional sediment mixing (Jacobs and Roberts, 2007; Roberts et al., 2015). We also measured all samples using the same GM-25-5 beta counter and OSL equipment and irradiated the grains using the same laboratory radiation source; all the data were analyzed by a single operator using a common set of procedures (a subset of the samples was cross-checked for operator bias). By holding constant all of these experimental variables for all samples, it was possible to remove much of the unwanted 'noise' in OSL data that typically prevents high-resolution ages from being obtained. In addition, the sources of error that apply to all samples (i.e., systematic errors) could be removed using this systematic approach, allowing all ages to be placed on the same calibrated timescale with improved precision (e.g., Jacobs et al., 2008). For purposes of comparison we have, therefore, used the random errors only and these are provided in brackets in Tables 2, 3 and 4. We have plotted the three stratigraphic profiles of the sites together with the OSL ages for all samples in Fig. 18 where we used different colors to indicate age equivalence or not. We

also summarized our proposed correlations based only on chronology in Table 6, together with the corresponding marine isotope stages.

The oldest dated deposits are found only at Pech II in Layers 6–9 (below the large cryoclastic deposit represented by Layer 5) and are indicated in purple in Fig. 18. These deposits date to between ~140 and 180 ka, falling within the penultimate glacial period, MIS 6; the associated lithic assemblages were assigned to the Clactonian and Acheulian by Bordes (1972). We have not plotted these ages in Fig. 18 for clarity, but they are provided in Table 3. We did not directly date Layer 5, but it likely relates to the penultimate glacial maximum at ~ 132 ka, and this is supported by a number of ESR ages on tooth enamel.

The first dated intact deposit in Fig. 18 is from Pech II in Layer 4D for which we obtained an age of 105 ± 7 ka (MIS 5d). This suggests either that the Pech sites were not occupied during the last interglacial (MIS 5e) or that no evidence for occupation at this time is preserved at any of the three sites (perhaps having been washed out of the sites). Significant flowstone deposits can be found in the tunnel between Pech I and Pech II and these have been dated to MIS 5e at ~125 ka (Schwarcz and Blackwell, 1983), and a post-depositional flowstone into the cryoclastic deposit in Layer 5 can also be seen. It is also evident from thin sections of Layer 4D that water might have washed out the fine fraction, providing further support that water action was at work in at least Pech II. The absence of evidence, therefore, does not necessarily demonstrate the presence of a sediment hiatus at Pech II.

The age for Layer 4D (105 ± 7 ka) is statistically consistent with the two ages for Layer 4B (80 ± 6 and 90 ± 6 ka; MIS 5b/c) and also the weighted mean age of 95 ± 4 ka (MIS 5c) for six samples from Layer 8 in Pech IV. This correlation is shown in green in Fig. 18. The ages for Layers 4B and 4D from Pech II bracket Layer 4C that Bordes thought was equivalent to Layer X (=Layers 7 and 8) in Pech IV based on typological similarities. Our correlations, thus, support his, even though it is older than he anticipated (e.g., he placed it in Würm I, roughly equivalent to later MIS 5). He also suggested that the archaeological assemblage in Layer 4B in Pech II, a Denticulate Mousterian, had no equivalent in Pech IV. Our ages for Layer 4B suggest that it might be a little later than Layer 4C/4D (Pech II) and Layer 8 (Pech IV), but we do not have the precision to resolve the difference statistically.

In Pech IV there is no evidence for occupation or sediment deposition during MIS 5b between ~90 and 80 ka (Figs. 13 and 14). Pech IV is then re-occupied again at the end of MIS 5a at ~77 ka in Layer 6B and shows continuous sediment deposition with sparse archaeological evidence throughout MIS 4 in Levels 6A, 5A, 5B and 4C (shown in yellow in Fig. 18). There is no chronological parallel in Pech II where the age hiatus suggests no sediment deposition during MIS 4. Bordes (1978) explicitly mentioned that his Pech IV Layers J3a-J3c (corresponding to Layers 6A and 6B in the recent excavations) containing the Asinipodian are very different from anything seen in Pech I or Pech II, and this is supported by our finding of no age equivalent in these other two sites.

It is only at the start of MIS 3 at ~60 ka that chronological parallels can again be drawn between Pech II and Pech IV (shown in blue in Fig. 18). Age estimates for Layers 4A, 3, 2G and 2F at Pech II are indistinguishable from each other at 58 ± 4 ka (Layer 4A), 61 ± 5 ka (Layer 3), and 60 ± 3 ka (Layer 2G; see Table 3). We did not obtain any age estimates for Layers 2A-2F at Pech II; Layers 2A-2C were not present in the profile we sampled and Layers 2D to 2F were very friable and full of

large limestone spalls (Fig. 3d and e). Electron spin resonance ages for Layer 2A and 2E (Fig. 14), however, are indistinguishable from each other and from ages for Layers 2F and 2G (Fig. 14; Grün et al., 1991). Bordes also noted that Layer 2 contained very little archaeological material. Layer 2G was archaeologically the densest part of Layer 2, but still contained very few lithics (*n*=91; Bordes 1972). We thus treat all of Layers 2, 3 and 4A as age equivalent deposits. These deposits are comparable to the ages obtained for Pech IV Levels 4A (57 ± 3 ka) and 4B (62 ± 3 ka; Table 4). Our correlations are shown in blue in Fig. 18, and, thus, differ from Bordes' correlation of the entire Pech II Layer 2 (A-G') to Pech IV Levels 4A through to 6B (see Table 5). As discussed above, Layers 4C, 5 and 6 at Pech IV have no age parallels at Pech II. Interestingly, though the assemblages are small, Bordes described Pech II Layer 2 as having Levallois flakes but also Quina type scrapers. He called these layers Ferrassie type Mousterian (Bordes, 1972). Layer 4A (Pech II) also had very few artifacts but Bordes (1972) noted that scrapers were frequent enough that he classified it as Typical Mousterian. The stratigraphically intermediate Layer 3 had more artifacts, no Quina type scrapers, and a moderate amount of Levallois production. At Pech IV, Layer 4 has a high percentage of scrapers with transverse forms (i.e., scrapers more common in Quina type Mousterian assemblages) becoming more common through the layer and with Levallois production steadily decreasing. Additionally, Layers 4B and 4C (at the top of 4) at Pech IV have very low artefact densities, so much so that Bordes (1975) called 4A only Mousterian and 4B Typical Mousterian with a question mark. Further, Level 4A at Pech IV had a number of archaeological horizons within it that appear to match the structure described for Layer 2 of Pech II, which was divided into eight levels. Thus, at both Pech II and IV the lithic assemblages seem to be similarly structured in this time window with frequent layers with low artefact densities, with scrapers being relatively common, with the presence of Levallois (decreasing at Pech IV) and the presence of scraper types typically associated with the Quina Mousterian.

Pech I and Pech IV show chronological overlap at the top of their respective archaeological sequences (shown as pink in Fig. 18) and the archaeological assemblages in both these sites belong to the MTA. We obtained identical ages at both sites and dated the MTA to ~51 ka in MIS 3. This supports the correlation drawn by Bordes (1972) (Table 5). Also, Bordes (1972) did not identify any MTA at Pech II, and in our chronology we see no occupation at Pech II during the MTA time period of Pech I and IV. We could not resolve the ages of the MTA-A and MTA-B, suggesting that in these sites the duration of these two assemblage types is probably shorter than the uncertainties associated with our ages. If the MTA is a chronological phase in southwest France, then at Pech IV the start of the MTA is constrained by the underlying Quina Mousterian dated to ~58 ka.

Conclusions

The archaeological sequences at Pech de l'Azé provide insights into the timing and nature of the Mousterian in southwestern France during the Late Pleistocene. By dating individual grains of quartz, we have been able to construct a detailed and reliable chronology for all three sites (Pech I, II and IV) that are consistent with, and support, the previous TL, ESR and, to some extent, the ^{14}C chronologies. The advantage of the new single-grain OSL chronology is that it provides a linked temporal framework for the vast majority of layers and levels in all three sites, and due to the systematic study design these new ages are directly comparable at a higher temporal resolution. None of the sites was occupied continuously nor preserves a complete and continuous sedimentary record. There is no archaeological overlap linking all three sites. There is some chronological overlap

between Pech I and IV, and between Pech II and IV, but none between Pech I and II, even though the latter two sites are situated adjacent to each other and separated only by a karstic tunnel. Together, the three sites contain four of the five classically defined Mousterian variants, namely the MTA (Pech I and IV), Quina Mousterian (Pech II and IV), Typical Mousterian (Pech II and IV) and the Denticulate Mousterian (Pech II), as well as the more recently defined Asinipodian from Pech IV. The single-grain OSL chronologies constructed for these three sites suggest that, at least locally, these variants form a time sequence. To some extent this conclusion could be seen as contrasting the recent suggestions of Guibert et al. (2008) and Richter et al. (2013), whose results supported an emerging pattern of considerable temporal overlap among the different Mousterian variants. One possible explanation of the lack of patterning in their data could simply be an artifact of using dates obtained by a variety of techniques and at different laboratories, which was much more controlled in the present study. However, it is important to bear in mind that the sequence of occupations at the various Pech de l'Azé sites may also reflect a very localized history of the occupation or use of these three locales more or less simultaneously, even though each site was individually affected by different site formation processes. Thus, while the temporal patterning seen here is interesting – especially in terms of what it says about scale of human occupations during the Middle Paleolithic – the history of occupation at this specific spot cannot be extended automatically to the wider region. In this sense, these results neither confirm nor deny the hypothesis of temporal ordering of the Mousterian industrial variants.

Acknowledgements

This research was funded by the Australian Research Council through Discovery Project grant DP1092843 to Jacobs, Dibble, Hublin and McPherron. We would like to specially thank The National Museum at Les Eyzies and its Director, Dr Cleyet-Merle, Dr Alain Turq and the Pech IV property owner, Mr LaPlanche. Sam Lin assisted with the survey to get accurate locational information for the OSL samples. Yasaman Jafari and Terry Lachlan helped with all aspects of the OSL dating program. We also thank all members of the excavation and research teams for valuable information that has helped us to understand and interpret the OSL data. We acknowledge the constructive reviews of three anonymous referees.

References

Aitken, M. J., 1985. Thermoluminescence Dating. Academic Press, London.

Aitken, M.J., 1998. An Introduction to Optical Dating. Oxford University Press, Oxford.

Ballarini, M., Wintle, A.G., Wallinga, J., 2006. Spatial variation of dose rates from beta sources as measured using single grains. Ancient TL 24, 1-8.

Bell, W.T., Zimmerman, D.W., 1978. The effect of HF acid etching on the morphology of quartz inclusions for thermoluminescence dating. Archaeometry 20, 63-65.

Bøtter-Jensen, L., Mejdahl, V., 1988. Assessment of beta dose-rate using a GM multicounter system. Nucl. Tracks Rad. Meas.14, 187-191.

Bøtter-Jensen, L., Bulur, E., Duller, G.A.T., Murray, A.S., 2000. Advances in luminescence instrument systems Radiat. Meas32, 523-528.

Bowman, S.G.E., Loosemore, R.P.W., Sieveking, G.d.G., Bordes, F., 1982. Preliminary dates for Pech de l'Aze IV PACT. Revue du groupe européen d'études pour les techniques physiques, chimiques et mathématiques appliquées à l'archéologie 6, 362-369.

Bertran, P., Texier, J.-P., 1995. Fabric analysis: application to Paleolithic sites J. Archaeol. Sci.22, 521-535.

Binford, L., 1973 Interassemblage variability: The Mousterian and the functional argument. In: Renfrew, C. (Ed), The Explanation of Culture Change. Duckworth, London, pp. 227-254.

Bordes, F., 1954-55. Les gisements du Pech de l'Azé (Dordogne). I. Le Mousterien de tradition acheuléenne I et suite, avec une note paleontologique de J.Bouchud. L'Anthropologie 58-59, 401-432 and 401-438.

Bordes, F., 1969. Os percé moustérien et os grave acheuléen du Pech de l'Azé II. Quaternarian XI, 1-6.

Bordes, F., 1971 Physical evolution and technological evolution in man: a parallelism. World Archaeol. 3, 1-5.

Bordes, F., 1972. A Tale of Two Caves. Harper and Row, New York.

Bordes, F., 1975. Le gisement de Pech de l'Azé IV: Note préliminaire. Bull. Soc. Prehist. Fr. 72, 293–308.

Bordes, F., 1977. Time and space limits of the Mousterian. In: Canberra R.V.S. Wright (Ed.), Stone Tools as Cultural Markers., Prehistory and Material Culture Series No. 12. Humanities Press, Canberra, pp. 37-39.

Bordes, F., 1978. Typological variability in the Mousterian layers at Pech de l'Azé I , II and I V. J. Anthropol. Res. 34, 181-193.

Bordes F., Bourgon M., 1950. Le gisement du Pech de l'Azé-Nord : prise de date et observations preliminaries. BSPF 47, 381-383.

Bordes, F., Bourgon, M., 1951. Le gisement du Pech de l'Azé-Nord, campagnes 1950-1951: les couches inférieures à *Rhinoceros mercki*. BSPF 48, 520-538.

Bordes, F., Prat, F., 1965. Observations sur les faunes du Riss et Würm I en Dordogne. L'Anthropologie 69, 31-45.

Bowman, S.G.E., Sieveking, G.D.G., 1983. Thermoluminescence dating of burnt flint from Combe Grenal. PACT, 9, p. 253-268.

Capitan, L., Peyrony, D., 1909. Deux squelettes humains au milieu de foyers de l'epoque mousterienne. Revue de l'Ecole d 'Anthropologie, 402-409

Delagnes, A., Rendu, W., 2011. Shifts in Neandertal mobility technology and subsistence strategies in western France. J. Archaeol. Sci. 38, 1771-1783.

Dibble, H.L., Raczek, T.P., McPherron, S.P., 2005. Excavator bias at Pech de l'Azé IV, France. J. Field Archaeol. 30, 317-328.

Dibble, H.L., McPherron, S.P., 2006 The Missing Mousterian. Current Anthropology 47, 777-803

Dibble, H., Berna, F., Goldberg, P., McPherron, S., Mentzer, S., Niven, L., Richter, D., Théry-Parisot, I., Sandgathe, D., Turq, A., 2009. A preliminary report on Pech de l'Azé I V, Layer 8 (Middle Paleolithic,France). PaleoAnthropology, 182-219.

Discamps, E., 2014. Ungulate biomass fluctuations endured by Middle and Early Upper Paleolithic societies (SW France, MIS 5-3): The contributions of modern analogs and cave hyena paleodemography. Quatern. Int.337, 64-79.

Discamps, E., Jaubert, J., Bachellerie, F., 2011. Human choices and environmental constraints: deciphering the variability of large game procurement from Mousterian to Aurignacian times (MIS 5-3) in southwestern France. Quaternary Sci. Rev. 30, 2755-2775.

Duller, G.A.T., 2003. Distinguishing quartz and feldspar in single grain luminescence measurements. Radiat. Meas. 37, 161-165.

Duller, G.A.T., 2004. Luminescence dating of Quaternary sediments: recent advances. J. Quaternary Sci. 19, 183-192.

Duller, G.A.T., 2007. Assessing the error on equivalent dose estimates derived from single aliquot regenerative dose measurements. Ancient TL 25, 15-24.

Falguères, C., Bahain, J.-J., Saleki, H., 1997. U-Series and ESR dating of teeth from Acheulian and Mousterian levels at La Micoque (Dordogne, France). J. Archaeol. Sci. 24, 537-545.

Galbraith, R.F., 2003. A simple homogeneity test for estimates of dose obtained using OSL. Ancient TL 21, 75-77.

Galbraith, R.F., Roberts, R.G., Laslett, G.M., Yoshida, H., Olley, J.M., 1999. Optical dating of single grain and multiple grains of quartz from Jinmium rock shelter, Northern Australia: Part I, experimental design and statistical models. Archaeometry 41, 339-364.

Goldberg, P., 1979. Micromorphology of Pech de l'Azé II : sediments. J. Archaeol. Sci. 6, 17-47.

Goldberg, P., Dibble, H., Berna, F., Sandgathe, D., McPherron, S.J.P., Turq, A., 2012. New evidence on Neandertal use of fire: Examples from Roc de Marsal and Pech de l'Azé IV. Quatern. Int. 247, 325-340.

Grün, R., Mellars, P, Laville, H., 1991. ESR chronology of a 100,000 year archaeological sequence at Pech de l'Azé II (France). Antiquity 65, 544-551.

Grün, R., Yan, G., MCculloch, M., Mortimer, G., 1999. Detailed mass spectrometric U-series analyses of two teeth from the archaeological site of Pech de l'Azé II : Implications for uranium migration and dating. J. Archaeol. Sci. 26, 1301-1310.

Guérin, G., Mercier, N., Adamiec, G., 2011. Dose-rate conversion factors: update. Ancient TL 29, 5-8.

Guérin, G., Discamps, E., Lahaye, C., Mercier, N., Guibert, P., Turq, A., Dibble, H.L., McPherron, S.P., Sandgathe, D., Goldberg, P., Jain, M., Thomsen, K., Patou-Mathis, M., Castel, J., Soulier, M., 2012. Multi-method (TL and OSL), multi-material (quartz and flint) dating of the Mousterian site of Roc de Marsal (Dordogne, France): correlating Neanderthal occupations with the climatic variability of MIS 5-3. J. Archaeol. Sci. 39, 3071-3084.

Guérin, G., Frouin, M., Talamo, S., Aldeias, V., Bruxelles, L., Chiotti, L., Dibble, H.L., Goldberg, P., Hublin, J.-J., Jain, M., Lahaye, C., Madelaine, S., Maureille, B., McPherron, S.J.P., Mercier, N., Murray, A.S., Sandgathe, D., Steele, T.E., Thomsen, K.J., Turq, A., 2015. A multi-method luminescence dating of the Palaeolithic sequence of La Ferrassie based on new excavations adjacent to the La Ferrassie 1 and 2 skeletons. J. Archaeol. Sci. 58, 147-166.

Guibert, P., Bechtel, F., Schvoerer, M., 1997. Déséquilibre des séries de l'uranium, implications sur la dose annuelle en datation par thermoluminescence : une étude à la grotte XVI, Cénac et Saint-Julien, Dordogne, France. Quaternaire 8, 377-389.

Guibert, P., Bechtel, F., Schvoerer, M., Rigaud, J.-Ph., Simek, J.-F., 1999. Datation par thermoluminescence de sediments chauffés provenant d'une aire de combustion moustérienne (Grotte XVI, Cénac et St-Julien, Dordogne, France). Revue d'Archéométrie 23, 163-175.

Guibert, P., Bechtel, F., Bourguignon, L., Brenet, M., Couchoud, I., Delagnes, A., Delpech, F., Detrain, L., Duttine, M., Folgado, M., Jaubert, J., Lahaye, C., Lenoir, M., Maureille, B., Texier, J.-P., Turq, A., Vieillevigne, E., Villeneuve, G., 2008. Une base de données pour la chronologie du Paléolithique moyen dans le Sud-Ouest de la France. In: Jaubert, J., Bordes, J.-G., Ortega, I., (Eds.), 2008. Les Sociétés du Paléolithique dans un Grand Sud-Ouest de la France: Nouveaux Gisements,Nouveaux Résultats, Nouvelles Méthodes, vol. 47. Sociéte préhistoriques française Bordeaux, pp. 19-40.

Higham, T., 2011. European Middle and Upper Palaeolithic radiocarbon dates are often older than they look: problems with previous dates and some remedies. Antiquity 85, 235-249.

Hublin, J.-J., Talamo, S., Julien, M., David, F.,Connet, N., Bodu, P., Vandermeersch, B., Richards, M.P., 2012. Radiocarbon dates from the Grotte du Renne and Saint-Césaire support a Neandertal origin for the Châtelperronian. Proc. Natl. Acad. 109, 18743-18748.

Huntley, D.J., Godfrey-Smith, D.I., Thewalt, M.L.W., 1985. Optical dating of sediments. Nature 313, 105–107.

Jacobs, Z., Roberts, R.G., 2007. Advances in optically stimulated luminescence dating of individual grains of quartz from archeological deposits. Evol. Anthropol 16, 210-223.

Jacobs, Z., Roberts, R.G., 2015. An improved single grain OSL chronology for the sedimentary deposits from Diepkloof Rockshelter, Western Cape, South Africa. . J. Archaeol. Sci. 63, 175-192.

Jacobs, Z., Duller, G.A.T., Wintle, A.G., 2006a. Interpretation of single grain D_e distributions and calculation of D_e. Radiat. Meas. 41, 264-277.

Jacobs, Z., Roberts, R.G., Galbraith, R.F., Deacon, H.J., Grün, R., Mackay, A., Mitchell, P., Vogelsang, R., Wadley, L., 2008. Ages for the Middle Stone Age of Southern Africa: Implications for human behavior and dispersal. Science 322, 733-735.

Jaubert, J., Bordes, J.-G., Discamps, E., Gravina, B., 2011. A new look at the end of the Middle Palaeolithic sequence in southwestern France. In: Derevianko, A.P., Shunkov, M.V. (Eds.), Characteristic Features of the Middle to Upper Paleolithic Transition in Eurasia. Asian Palaeolithic Association, Novosirbirsk.

Jaubert, J., 2012. Les archéo-sequences du Paléolithique moyen du Sud-Ouest de la France: quel bilan un quart de siècle après François Bordes. In In F. Delpech and J. Jaubert (Eds.) François Bordes et La Préhistoire. Éditions du Comité des travaux historiques et scientifiques, 29, 235-253.

Jones, H.L., 2001. Electron Spin Resonance (ESR) dating of tooth enamel at three Palaeolithic archaeological sites. M.Sc. thesis, McMaster University.

Lahaye, C., 2005. Nouveaux apports de la thermoluminescence à la chronologie du Paléolithique dans le Sud-Ouest de la France. Études en milieu hétérogène et en présence de déséquilibres radioactifs dans les séries de l'uranium. Ph.D. Dissertation, Université Bordeaux 3..

Laquay, G., 1981. Recherches sur les faunes du Würm I en Périgord, Thèse de 3e cycle, Université de Bordeaux 1.

Lartet, E., Christy H., 1864. Cavernes du Périgord. Revue Archéol. 1, 233-267.

Laville, H., 1975. Climatologie et chronologie du paléolithique en Périgord: Etude sédimentologique de depots en grottes et sous abris. Thèse Doctorate d'État. Marseilles: Université de Provence.

Laville, H., 1973. The relative position of Mousterian industries in the climatic chronology of the Early Würm in the Périgord. World Archaeol. 4, 323-329.

Laville, H ., Rigaud, J.-P., Sackett J., 1980. Rock Shelters of the Perigord : Geological Stratigraphy and Archaeological Succession. Academic Press, New York.

Lian, O.B., Roberts, R.G., 2006. Dating the Quaternary: progress in luminescence dating of sediments. Quaternary Sci. Rev. 25, 2449-2468.

McPherron, S., Dibble, H.L., 2000. The lithic assemblages of Pech de l'Azé IV (Dordogne, France). Préhistoire Européenne 15, 9–43.

McPherron, S., Soressi, M., Dibble, H., 2001. Deux nouveaux projets de recherché à Pech de l'Azé (Dordogne, France). Préhistoire du Sud-Ouest 8, 11-30.

McPherron, S., H. Dibble, P. Goldberg, M. Lenoir, D. Sandgathe, and A. Turq. 2012a. De Combe Grenal À Pech de l'Azé IV: L'Evolution Des Méthodes de Fouilles de François Bordes. In F. Delpech and J. Jaubert (Eds.) François Bordes et La Préhistoire. Éditions du Comité des travaux historiques et scientifiques 29, 65-77.

McPherron, S.P., Talamo, S., Goldberg, P., Niven, L., Sandgathe, D., Richards, M.P., Richter, D., Turq, A., Dibble, H.L., 2012b. Radiocarbon dates for the late Middle Palaeolithic at Pech de l'Azé IV, France. J. Archaeol. Sci. 39, 3436-3442.

Mejdahl, V., 1979. Thermoluminescence dating: beta-dose attenuation in quartz grains. Archaeometry 21, 61–72.

Mellars, P.A., 1965. Sequence and development of the Mousterian traditions in Southwestern France. Nature 205, 626-627.

Mellars, P.A., 1969. The chronology of Mousterian industries in the Périgord region of southwest France. Proc. Prehist. Soc. 35, 134-171.

Mellars, P., 1970 Some comments on the notion of «functional variability» in stone-tool assemblages. World Archaeol. 2, 74-89.

Mellars, P., 1988. The chronology of the South-West French Mousterian: A review of the current debate. In: L. Binford & J.-P. Rigaud (Eds.), L'Homme de Neandertal -4- La technique, Liège, Etudes et Recherces Archéologiques de l'Université de Liège 31, p. 97-120.

Mellars, P., 1989 Technological changes across the Middle-Upper Palaeolithic transition: economic, social and cognitive perspectives. In: P. Mellars, P. Streinger, C. (Eds.), The Human Revolution Princeton University Press, Princeton, pp. 339-365.

Mellars, P., 1992 Technological changes in the Mousterian of Southwest France. In: H.L. Dibble & P.A. Mellars (Eds.) The Middle Paleolithic : adaptation, behaviour, and variability. Monograph of the University of Pennsylvania Museum, 78, The University Museum Press, Philadelphia, p. 29-43.

Mellars, P., Grün, R., 1991. A comparison of the electron spin resonance and thermoluminescence dating methods: the results of ESR dating at Le Moustier (France). Cambridge Archaeol. J. 1, 269-276.

Mercier, N., Falguères, C., 2007. Field gamma dose-rate measurement with a NaI(Tl) detector: re-evaluation of the 'threshold' technique. Ancient TL 25, 1-4.

Murray, A.S., Wintle, A.G., 2000. Luminescence dating of quartz using an improved single-aliquot regenerative-dose protocol. Radiat. Meas. 32, 57-73.

Olley, J.M., Murray, A., Roberts, R.G., 1996. The effects of disequilibria in the uranium and thorium decay chains on burial dose rates in fluvial sediments. Quaternary Sci. Rev. 15, 751-760.

Olley, J. M., Roberts, R. G., Murray, A. S., 1997. Disequilibria in the uranium decay series in sedimentary deposits at Allen's cave, Nullarbor plain, Australia: Implications for dose rate determinations. Radiat. Meas.27, 433-443.

Paquereau, M.M., 1969. Étude palynologique du Würm I du Pech de l'Azé (Dordogne). Quaternaria XI, 227-235.

Peyrony, D., 1925. Le gisement préhistorique du haut de Combe-Capelle. Moustérien de Tradition Acheuléen. Association Française pour l'Avancement des Sciences 49, 484-487.

Prescott, J.R., Hutton, J.T., 1994. Cosmic ray contributions to dose rates for luminescence and ESR dating: Large depths and long term time variations. Radiat. Meas. 23, 497-500.

Reimer, P.J., Bard, E., Bayliss, A., Beck, J.W., Blackwell, P.G., Bronk Ramsey, C., Buck, C.E., Cheng, H., Edwards, R.L., Friedrich, M., Grootes, P.M., Guilderson, T.P., Haflidason, H., Hajdas, I., Hatté, C., Heaton, T.J., Hoffmann. D.L., Hogg. A.G., Hughen, K.A., Kaiser, K.F., Kromer, B., Manning, S.W., Niu, M., Reimer, R.W., Richards, D.A., Scott, E.M., Southon, J.R., Staff, R.A., Turney, C.S.M., Van der Plicht, J., 2013. IntCal13 and Marine13 radiocarbon age calibration curves 0-50,000 years cal BP. Radiocarbon 55, 1869–1887.

Rhodes, E. J., Schwenninger, J.-L., 2007. Dose rates and radioisotope concentrations in theconcrete calibration blocks at Oxford. Ancient TL 25, 5-8.

Richter, D., Dibble, H., Goldberg, P., McPherron, S.P., Niven, L., Sandgathe, D., Talamo, S., Turq, A., 2013. The late Middle Palaeolithic in southwest France: New TL dates for the sequence of Pech de l'Azé IV. Quatern. Int. 294, 160-167.

Rittenour, T.M., 2008. Luminescence dating of fluvial deposits: applications to geomorphic, palaeoseismic and archaeological research. Boreas 37, 613-635.

Roberts, R.G., Jacobs, Z., Li, B., Jankowski, N.R., Cunningham, A.C., Rosenfeld, A.B., 2015 Optical dating in archaeology: Thirty years in retrospect and grand challenges for the future. J. Archaeol. Sci. 56, 41-60.Rolland, N., Dibble, H., 1990. A new synthesis of Middle Paleolithic variability. Am. Antiq. 55, 480-499.

Schwarcz, H.P., Blackwell,B., 1983. ^{230}Th/^{234}U age of a Mousterian site in France. Nature 301, 236-237.

Smith, M.A., Prescott, J.R., Head, M.J., 1997. Comparison of ^{14}C and luminescence chronologies at Puritjarra rock shelter, central Australia. Quaternary Sci. Rev. 16, 299-320.

Soressi, M., 2004. From Mousterian of Acheulian tradition type A to type B: technical tradition, raw material, task, or settlement dynamic changes? In: Conard, N.J. (Ed), Settlement Dynamics of the Middle Paleolithic and Middle Stone Age, vol. II. Tübingen Publications in Prehistory, Kems Verlag, pp. 343-366.

Soressi, M., d'Errico, F., 2007. Pigments, gravures, parures : les comportements symboliques controversés des Néandertaliens. In Vandermeersch, B. and Maureille, B., Les Néandertaliens. Biologie et cultures. Paris, Éditions du CTHS, 297-309.

Soressi, M., Jones, H.L., Rink, W.J., Maurille, B., Tillier, A.-M., 2007. The Pech de l'Azé I Neandertal child: ESR, uranium-series, and AMS ^{14}C dating of its MTA type B context. J. Hum. Evol. 52, 455-466.

Soressi , M., Rendu, W, Texier J.-P., Claud, E., Daulny, L., d'Errico, F., Laroulandie, V., Maureille, B., Niclot, M., Schwortz, S., Tillier, A.-M., 2008. Pech de l'Azé I (Dordogne, France) : nouveau regard sur un gisement moustérien de tradition acheuléenne connu depuis le XIXe siècle. In: J. Jaubert, J.-G. Bordes, I. Ortega (Eds.) Les sociétés Paléolithiques d'un grand Sud-Ouest : nouveaux gisements, nouvelles méthodes, nouveaux résultats. Société Préhistorique Française, Mémoire 47, pp. 95-132.

Soressi, M., McPherron, S.P., Lenoir, M., Dogandžić, T., Goldberg, P., Jacobs, Z., Maigrot, Y., Martisius, N., Miller, C.E., Rendu, W., Richards, M.P., Skinner, M.M., Steele, T.E., Talamo, S., Texier, J.-P., 2013. Neandertals made the first specialized bone tools in Europe. Proc. Natl. Acad. Sci. 110, 14186-14190.

Talamo, S., Soressi, M., Roussel, M., Richards, M., Hublin, J.-J., 2012. A radiocarbon chronology for the complete Middle to Upper Palaeolithic transitional sequence of Les Cottés (France). J. Archaeol. Sci. 39, 175-183.

Texier, J.-P., 2000. À propos des processus de formation des sites préhistoriques. Paléo 12, 379-386.

Texier, J.-P., 2009. Histoire Géologique de Sites Préhistoriques Classiques du Périgord: Une Vision Actualisée. Éditions du comité des travaux historiques et scientifiques, Paris.

Turq, A., Dibble, H.L., Goldberg, P., McPherron, S.P., Sandgathe, D., Jones, H., Maddison, K., Maureille, B., Mentzer, S., Rink, J., Steenhuyse, A., 2011. Les fouilles récentes du Pech de l'Azé IV (Dordogne).– Gallia Préhist. 53, 1-58.

Valladas, H., Geneste, J.-M., Joron, J.-L., Chadelle, J.-P., 1986. Thermoluminescence dating of Le Moustier (Dordogne, France). Nature 322, 452-454.

Valladas, H., Chadelle, J.-P., Geneste, J.-M., Joron, J.-L., Meignen, L., Texier, P.-J., 1987. Datations par la thermoluminescence de gisements moustériens du sud de la France. L'Anthropologie 91, 211-226.

Valladas, H., Mercier, N., Falgueres, C., Bahain, J.-J., 1999. Contribution des méthodes nucléaires à la chronologie des cultures paléolithiques entre 300 000 et 35 000 ans BP. – Gallia Préhist. 41, 153-166.

Valladas, H., Mercier, N., Joron, J.-L., McPherron, S. P., Dibble, H. L., Lenoir, M., 2003. TL dates for the Middle Paleolithic site of Combe-Capelle Bas, France. J. Archaeological Science 30, 1443-1450.

Vieillevigne, E., Bourguignon, L., Ortega, I., Guibert, P., 2008. Analyse croisée des données chronologiques et des industries lithiques dans le grand sud-ouest de la France (OIS 10 à 3). Paléo 20, 145–165.

Vogel, J.C., Waterbolk,T., 1967. Groningen radiocarbon dates VII. Radiocarbon 9, 107-155.

Wintle, A.G., 1997. Luminescence dating: Laboratory procedures and protocols. Radiat. Meas. 27, 769-817.

Wintle, A.G., 2008. Fifty years of luminescence dating. Archaeometry 50, 276-312.

Figure captions

Figure 1: a) Map of France indicating the location of the Department of the Dordogne in southwest France. b) A map of the Dordogne area showing the location of several important sites relative to known cities. 1 Pech de l'Azé, 2 Combe Grenal, 3 Combe Capelle Bas, 4 Abri Peyrony, 5 Roc de Marsal, 6 La Ferrassie, 7 Le Moustier. c) Schematic of the limestone cliff and the position of the three Pech sites (after Soressi et al., 2008).

Figure 2: a) Planform map of the different excavations conducted at Pech I. The two areas of interest in this study is the witness section outlined in yellow and the Capitan and Peyrony excavation. The yellow star indicates the relative position from where the juvenile Neandertal baby skull and jaw were found. b) Photograph of the witness section. c) Schematic of the witness section showing the locations of the OSL samples (black filled circles) and gamma spectrometry holes (open red circles) of Rink, reported in Soressi et al. (2007). d) Close-up photograph showing the location of the OSL samples removed from the collapsed cave wall left-over from, and directly related to the Capitan and Peyrony excavation.

Figure 3: a) Planform map of Pech II, showing the location of the three profiles from which OSL samples were collected. b) Photograph of Profile B and the location of the OSL samples. C) Photograph of Profile C and the location of the OSL samples. d) Stratigraphic drawing of part of Profile A with the OSL sample locations indicated, together with the layer numbers following Bordes (1972) in the left-hand column and Texier (2009) in the right-hand column. e) Photograph of the profile in d) with the locations of the OSL samples. The red boxes denote the position of the OSL samples. The black filled circles show the position of the gamma spectrometry measurements.

Figure 4: a) Planform map of Pech IV. The red rectangles indicate the two squares from which all OSL samples were collected. b) Stratigraphic drawing of the west profile showing the layer numbers and relative depth of the deposit. c) Photograph of the north profile from which the majority of the OSL samples were collected together with the layer number and sample numbers. d) Photograph of the west profile from which all OSL samples from Layer 8 were collected. The red filled circles indicate the OSL samples, whereas the red rectangle indicates the block samples that were later sub-sampled for OSL dating in the lab. The white lines denote the areas sub-sampled and their corresponding sample names.

Figure 5: Radial plots of single-grain D_e distributions for a representative samples measured from a) Pech 1, b) Pech II and c) Pech IV. If the D_e estimates in each distribution were statistically consistent (at 2σ) with a common value, then 95% of the points should fall within any grey band projecting ± 2 units from the standardised estimate axis and the overdispersion (OD) should be consistent with 0%. The grey band is centered on the CAM weighted mean D_e value.

Figure 6: Comparison of the in situ gamma dose rate results obtained from two different laboratories a decade apart. The gamma dose rate measurements were made in the same holes.

Figure 7: Pech I - The ratio of beta dose rates obtained for the same samples using three different methods. The filled circles show the ratio of the results obtained from ICP-MS(OES) and GM-25-5 beta counting. The filled squares show the results obtained from TSAC and XRF against GM-25-5 beta counting and the filled triangles show the results obtained from ICP-MS(OES) against TSAC and XRF. The samples are plotted in stratigraphic order and per layer for the witness section (Fig. 2c) and separately for the samples collected from the cave wall (Fig. 2d).

Figure 8: Pech II - The ratio of beta dose rates obtained for the same samples using three different methods. The filled circles show the ratio of the results obtained from ICP-MS(OES) and GM-25-5 beta counting. The filled squares show the results obtained from TSAC and XRF against GM-25-5 beta counting and the filled triangles show the results obtained from ICP-MS(OES) against TSAC and XRF. The samples are plotted in stratigraphic order and the corresponding layer name is noted.

Figure 9: Gamma dose rate results for sediment from Pech IV using an in situ gamma spectrometer (this study) or α- Al_2O_3:C dosimeters (Richter et al., 2013). The results are not for exactly the same position and measurements were made for different profiles in the site. The average for each layer and for each method is provided in the boxes and shown on top of each box is the ratio of the two averages.

Figure 10: a) Pech IV - The ratio of beta dose rates obtained from ICP-MS (U and Th) and ICP-OES (K) and GM-25-5 beta counting plotted in stratigraphic order and the layers are demarcated. The broken vertical line indicated unity. b) Uranium concentrations (ppm) obtained from ICP-MS measurements plotted for all samples and in stratigraphic order.

Figure 11: a) All ages for Pech I plotted in stratigraphic order with the layers demarcated with stippled lines. The filled symbols represent ages for samples collected from the witness section (Fig. 2c) and the open symbol those samples collected from the cave wall (Fig. 2d). The broken vertical line shows the weighted mean age calculated for all 19 samples and the gray shaded bar the 1σ standard error on the weighted mean. b) The weighted mean ages for each layer. The weighted mean ages include all samples from the witness section and the cave wall. Weighted mean ages were calculated using three different beta dose rates (open circles—GM-25-5 beta counting, open triangles—TSAC+XRF and open squares—ICP-MS and ICP-OES). The same weighted mean and 1σ standard error as in a).

Figure 12: All OSL ages for Pech I together with all independent ages published previously for Pech I, shown per layer. Ages are plotted with 1σ uncertainties. The EU and LU ages are plotted as a range and the ^{14}C ages are plotted where the line is the midpoint value of the calibrated range and the error bars represent the entire range. The broken line is the weighted mean age calculated for all the OSL ages and the stippled lines are the 1σ standard error on the weighted mean age.

Figure 13: All ages for Pech II plotted in stratigraphic order with the layers demarcated with stippled lines. All samples from Layers 2G to 4D were collected from Profile A in Fig. 3a, d and e, and samples from Layers 7A to 9 are for samples collected from Profiles B and C (Fig. 3b and c) below the large cryoclastic deposit in Layer 5.

Figure 14: All OSL ages for Pech II together with the previously published ESR (EU and LU) and U-series ages. Ages are plotted with 1σ uncertainties. The EU and LU ages are plotted as a range. Each ESR age is the average of 2 to 4 different fragments of the same tooth (see Grün et al., 1991) for each individual age estimate. a) All ages for deposits above Layer 5 and b) all ages for deposits in Layer 5 and below.

Figure 15: a) All OSL age estimates with their 1σ errors for samples collected from Pech IV shown as a function of their depth below datum and in stratigraphic order with the layer boundaries demarcated. b) Weighted mean ages for each layer plotted as a function of their depth below datum. The stippled line is a two period moving average line fitted to the data. The two horizontal black marks indicate a break between layers 6 and 8 because the samples were not collected from the same stratigraphic profile.

Figure 16: a) Two sets of OSL ages plotted for the same samples from Pech IV. One set (filled circles) were calculated using GM-25-5 beta counting for estimation of the beta dose rate, whereas the other set (open triangles) used ICP-MS measurements for beta dose rates instead. Uncertainties are not shown for clarity. Uncertainties for ages shown as filled circles are provided in Table 4 and for ages shown as open triangles, the errors range between 6.5 and 11.5% at 1σ. b) Ratio of the two age estimates plotted in a). The broken line indicates unity.

Figure 17: All OSL ages for Pech IV together with all independent ages published previously for Pech IV, shown per layer. Ages are plotted with 1σ uncertainties. The EU and LU ages are plotted as a range and the ^{14}C ages are plotted where the line is the midpoint value of the calibrated range and the error bars represent the entire range. The ^{14}C ages were calibrated using IntCal13 (Reimer et al., 2013).The broken line is the weighted mean age calculated for all the OSL ages in a layer and the stippled lines are the 1σ standard error on the weighted mean age. The red stippled line indicates the 2σ standard error on the weighted mean age for layer 3A and B.

Figure 18: Composite figure of all three sites indicating where there is overlap with regards to age (shown as the same color; pink, blue and green), where deposits are represented in only one site (yellow and purple) and those parts of the sequences that remains undated (shown in gray). We omitted the ages for the deposits below cryoclastic layer in Pech II (shown in purple) for clarity, but these ages are provided in Table 3. Also shown are the Marine Isotope Stages (MIS) for comparison with Table 6.

Table

Stratigraphy	Archaeological Industry	Sedimentology
7	MTA-B	Sandy-clayey matrix; large limestone fragments; voids due to biological activity; carbonate features including calcite impregnation of sediment
6	MTA-B	
5	MTA-A/B	Sandy, slightly clayey sediment matrix; limestone fragments, flint and bone; bone and charcoal less abundant than in layer 4; biological activity in the form of root channels, earthworm casts and mite pellets; some biological voids filled post-depositionally with fine sands.
4	MTA-A	Poorly sorted silty-clayey sand; some limestone fragments, flint, burnt and unburnt bone and traces of charcoal. Clear combustion features towards the south. Sediments are bedded, suggesting no significant post-depositional vertical movement of objects
3	MTA-A	Yellow sand; ash lenses
2	Sterile	Pavement of flat limestone slabs
1	Sterile	Light yellow fluvial sand; some small rock fragment near the top of the layer

Table 1a: Summary of the stratigraphic layers and archaeological industries found at Pech I. Also given is a short synopsis of the most important sedimentological information for each layer. MTA – Mousterian of the Acheulian Tradition.

Stratigraphy (Bordes, 1972; Laville, 1973)	**Stratigraphy** (Texier, 2009)	**Archaeological Industry (Bordes, ?)**	**Sedimentology**
S			Modern soil, disturbed by rodents
1		Indeter.	Reddish sandy layer with small archaeological traces
2A	4	Ferrassie-type Mousterian (Levallois flakes and Quina-type scrapers)	Yellow sands with limestone fragments
2B			
2C			
2D			Sandy clay with rare limestone fragments
2E			Brown, clayey, silty sand; numerous limestone fragments with sharp edges; smaller rock fragments
2F			Clayey, silty sand; with smaller flat limestone fragments
2G1			Slightly clayey sand with fine rock fragments; scattered limestone fragments in sands
2G2			Slightly clayey sand; discontinuous large and relatively rounded rock fragments
2G3			Clayey sand with small limestone fragments; very friable.
3		TM	Light brown, sandy-clay matrix; some limestone fragments
4A		TM	Reddish-brown, sandy clay, with rare limestone fragments. Some traces of fire
4B		Denticulate Mousterian	Red–brown, sandy-clay; very hard when dry; numerous traces of fire
4C		TM	Alternation of clay-like sands and brown clay; numerous traces of fire
4D		TM	Clayey-sand matrix; small rounded rock fragments
5	3	Sterile	Cryoclastic complex; thick layer of large rock fragments, fining upwards; archaeologically almost sterile; stalagmite fragments throughout.
6	2	Clactonian	Brown–red sandy, silty clay; altered rock fragments and clay coatings
7A		Clactonian	Brown sand with some clay; limestone fragments are rare
7B		Clactonian	Yellow–brown sand; more clay than in 7A; some rounded rock fragments.
8		Clactonian	Thin reddish silt (palaeosol (?)); brown, clayey sand; well rounded rock fragments.
9		Acheulean	Brown sand, clayey in some areas where not cemented; rounded limestone fragments
10	1	Sterile	Sterile cross-bedded and horizontal fluvial sand; some rounded gravel and iron rich pebbles.

Table 1b: Summary of the stratigraphic layers and archaeological industries found at Pech II. Also given is a short synopsis of the most important sedimentological information for each layer. Information on the archaeological industries was taken from Bordes (1972) and for the sedimentology from Bordes (1972), Laville (1972) and Goldberg (1979). TM – Typical Mousterian.

Stratigraphy	Archaeological Industry	Sedimentology
1	None	Part of modern soil profile. Dark brown, organic rich silty to sandy layers with rounded and dissolving limestone fragments.
2	None	Spatially restricted unit of rounded pebbles, and limestone fragments in a sandy, silty matrix.
3A	MTA-B	Red/yellow silty-sand with limestone fragments more compacted and less cemented than underlying layer 4. Limestone fragments are rounded and appear to be dissolved.
	MTA-A/B	
3B	MTA-A	Red/yellow silty-sand with limestone fragments more compacted and less cemented than underlying layer 4. Limestone fragments are rounded and appear to be dissolved.
4A	Quina	Red/yellow silty-sand with limestone fragments. Strongly cemented with calcite in some regions produced a breccia.
4B	TM	Red/yellow silty-sand with greater concentration of limestone fragments than the overlying 4A layer.
Vault collapse		Limestone slabs and blocks
4C	TM	Silty-sand with higher concentrations of small eroded limestone fragments and bone fragments.
5A	TM	Red/yellow silty-sand with angular limestone blocks
5B		Red/yellow silty-sand with limestone fragments, some of which are well-rounded.
6A	Asinipodian	Dark brown to red/yellow silty-sand with large block of limestone occurring in the upper portion
6B		Silty-sand with varying sizes of limestone blocks
Roof collapse		Limestone slabs and blocks
7	?Mousterian	Thin layer of coarse sand with edge damaged stone tools.
8	Typical Mousterian	Black, bedded clayey-sand with major organic anthropogenic component. Charcoal and ash lenses with burnt and unburnt bone fragments.

Table 1c: Summary of the stratigraphic layers and archaeological industries found at Pech IV. Also given is a short synopsis of the most important sedimentological information for each layer. All information was taken from Turq et al. (2011). MTA – Mousterian of the Acheulian Tradition; TM – Typical Mousterian.

Sample code	Moisture content (%)	Dose rates (Gy/ka)			Total dose rate (Gy/ka)	D_e (Gy)	Number of grains	Over-dispersion (%)	OSL age (ka)	*p*-value
		Beta	Gamma	Cosmic						
Level 7										
PdLI-7	7.4	0.53 ± 0.04	0.43 ± 0.02	0.10	1.09 ± 0.06	51.0 ± 1.9	62 / 1000	20 ± 3	46.8 ± 3.4 (2.8)	
PdLI-8	4.9	0.53 ± 0.04	0.36 ± 0.02	0.10	1.03 ± 0.06	52.6 ± 2.3	73 / 1000	31 ± 4	51.3 ± 3.8 (3.0)	
PdLI-9	1.3	0.46 ± 0.03	0.23 ± 0.01	0.10	0.82 ± 0.04	38.8 ± 2.0	47 / 1000	26 ± 5	47.2 ± 3.5 (3.0)	
PdLI-10	1.9	0.53 ± 0.03	0.26 ± 0.01	0.10	0.93 ± 0.05	46.1 ± 4.5	36 / 1000	53 ± 7	49.7 ± 5.5 (3.4)	
PdLI-11	3.3	0.58 ± 0.04	0.26 ± 0.01	0.10	0.97 ± 0.06	50.2 ± 2.4	55 / 1000	26 ± 4	51.8 ± 4.0 (3.2)	
							Weighted mean =		***49.2 ± 2.9*** (1.4)	*p* = 0.78
PdLI-3	0.5	0.56 ± 0.03	0.39 ± 0.06	0.08	1.06 ± 0.09	54.6 ± 2.8	64 / 1000	36 ± 4	51.7 ± 5.3 (4.6)	
PdLI-2	2.3	0.72 ± 0.04	0.34 ± 0.05	0.08	1.17 ± 0.09	55.4 ± 2.5	63 / 1000	30 ± 4	47.2 ± 4.3 (3.6)	
PdLI-5	3.6	0.75 ± 0.04	0.37 ± 0.06	0.08	1.22 ± 0.10	56.5 ± 3.0	61 / 1000	34 ± 4	46.3 ± 4.5 (3.9)	
							Weighted mean =		***48.0 ± 3.5*** (2.5)	*p* = 0.74
							Grand weighted mean =		***48.9 ± 2.8*** (1.2)	*p* = 0.83
Level 6										
PdLI-12	3.4	0.56 ± 0.04	0.31 ± 0.02	0.12	1.03 ± 0.05	54.7 ± 3.2	43 / 1000	25 ± 6	53.3 ± 4.3 (3.8)	
PdLI-13	2.4	0.54 ± 0.03	0.31 ± 0.02	0.13	1.01 ± 0.05	50.8 ± 3.2	46 / 1000	48 ± 7	50.4 ± 4.3 (3.6)	
PdLI-14	2.8	0.55 ± 0.04	0.34 ± 0.02	0.13	1.04 ± 0.05	56.9 ± 3.2	41 / 1000	38 ± 6	54.6 ± 4.3 (3.6)	
							Weighted mean =		***52.6 ± 3.0*** (2.2)	*p* = 0.71
PdLI-4	1.6	0.57 ± 0.03	0.30 ± 0.05	0.08	0.98 ± 0.08	51.8 ± 2.3	63 / 1000	40 ± 5	52.8 ± 4.9 (4.1)	
							Grand weighted mean =		***52.7 ± 3.0*** (2.0)	*p* = 0.88
Level 5										
PdLI-15	1.1	0.52 ± 0.03	0.36 ± 0.02	0.13	1.04 ± 0.05	54.7 ± 2.6	53 / 1000	33 ± 5	52.3 ± 3.8 (3.2)	
PdLI-16	1.0	0.55 ± 0.04	0.36 ± 0.02	0.13	1.07 ± 0.06	57.8 ± 3.1	57 / 1000	34 ± 4	53.8 ± 4.2 (3.5)	
PdLI-17	2.0	0.58 ± 0.04	0.54 ± 0.03	0.11	1.26 ± 0.06	68.0 ± 3.3	63 / 1000	31 ± 4	54.2 ± 3.9 (3.4)	
							Weighted mean =		***53.4 ± 2.9*** (2.1)	*p* = 0.94
PdLI-1	4.2	0.66 ± 0.04	0.35 ± 0.05	0.08	1.12 ± 0.09	58.2 ± 2.2	87 / 1000	30 ± 3	52.2 ± 4.9 (4.1)	
							Grand weighted mean =		***53.2 ± 2.9*** (1.9)	*p* = 0.96
Level 4										
PdLI-18	4.0	0.55 ± 0.03	0.63 ± 0.03	0.08	1.29 ± 0.07	67.6 ± 2.1	90 / 2000	17 ± 3	52.5 ± 3.4 (2.7)	
PdLI-19	3.6	0.48 ± 0.03	0.52 ± 0.03	0.08	1.11 ± 0.06	55.4 ± 1.4	126 / 1900	18 ± 3	50.0 ± 3.1 (2.5)	
PdLI-20	4.0	0.40 ± 0.03	0.36 ± 0.02	0.16	0.94 ± 0.05	48.4 ± 1.0	140 / 2000	16 ± 2	51.3 ± 3.1 (2.4)	
							Grand weighted mean =		***51.2 ± 2.4*** (1.5)	*p* = 0.80

Table 2: Dose rate data, equivalent doses and OSL ages for sediment samples from Pech-de-l'Azé I. Also provided are the weighted mean ages for each layer. The calculated *p*-values indicate the probability that a random value from a chi-squared distribution with n-1 degrees of freedom is greater than the homogeneity test statistic, G of Galbraith (2003). A small *p*-value (by convention <0.05) indicates that the ages are not all compatible with a common value.

Sample code	Layer	Moisture content (%)	Dose rates (Gy/ka)			Total dose rate (Gy/ka)	D_e (Gy)	Number of grains	Over-dispersion (%)	OSL age (ka)
			Beta	Gamma	Cosmic					
PdLII-5	2G1	1.9	0.63 ± 0.03	0.42 ± 0.02	0.07	1.15 ± 0.06	72.9 ± 2.9	113 / 2000	29 ± 3	63.3 ± 4.1 (3.2)
PdLII-6	2G1	8.3	0.67 ± 0.04	0.42 ± 0.02	0.07	1.19 ± 0.07	70.9 ± 3.1	118 / 2000	38 ± 4	59.4 ± 4.3 (3.5)
PdLII-8	2G1	3.1	0.71 ± 0.03	0.43 ± 0.02	0.07	1.24 ± 0.06	80.7 ± 2.8	123 / 2000	28 ± 3	65.3 ± 4.2 (3.2)
PdLII-11	2G2	3.1	0.91 ± 0.05	0.44 ± 0.02	0.07	1.45 ± 0.07	88.9 ± 3.3	118 / 2000	31 ± 3	61.5 ± 4.0 (2.9)
PdLII-13	2G2	2.1	0.63 ± 0.03	0.44 ± 0.02	0.07	1.16 ± 0.06	64.6 ± 1.3	410 / 2000	33 ± 2	55.7 ± 3.2 (2.2)
PdLII-14	3	2.0	0.88 ± 0.05	0.44 ± 0.02	0.07	1.42 ±0.07	86.1 ± 4.4	101 / 2000	45 ± 4	60.5 ± 4.5 (3.9)
PdLII-16	4A1	1.4	0.86 ± 0.04	0.52 ± 0.03	0.06	1.47 ± 0.07	84.8 ± 3.9	68 / 2000	25 ± 4	57.7 ± 4.0 (3.2)
PdLII-17	4B	1.4	0.81 ± 0.05	0.59 ± 0.03	0.06	1.49 ± 0.08	133.7 ± 4.9	110 / 2000	34 ± 3	89.9 ± 5.9 (4.7)
PdLII-18	4B	1.5	0.61 ± 0.03	0.50 ± 0.03	0.06	1.20 ±0.06	96.4 ± 4.3	100 / 2000	36 ± 4	80.3 ± 5.5 (4.6)
PdLII-19	4D	0.7	0.71 ± 0.04	0.41 ± 0.02	0.05	1.21 ± 0.06	135.4 ± 4.8	118 / 2000	24 ± 3	105.3 ± 6.8 (5.2)
PdLII-2	7A	2.8	0.73 ± 0.04	0.48 ± 0.02	0.02	1.26 ± 0.06	180.8 ± 6.5	70 / 2000	16 ± 4	143.3 ± 9.3 (7.1)
PdLII-4	7B	1.7	0.66 ± 0.04	0.48 ± 0.02	0.02	1.22 ± 0.06	192.6± 9.4	71 / 2000	30 ± 5	161.3 ± 11.9 (9.9)
PdLII-10	7B	7.0	0.50 ± 0.03	0.48 ± 0.02	0.02	1.03 ± 0.06	185.1 ± 7.6	78 / 2000	25 ± 4	179.0 ± 12.9 (11.8)
PdLII-12	7B	3.3	0.51 ± 0.03	0.41 ± 0.02	0.01	0.97 ± 0.05	169.8 ± 8.6	80 / 1900	35 ± 5	176.0 ± 13.7 (11.8)
PdLII-9	7B	3.1	0.75 ± 0.04	0.41 ± 0.02	0.01	1.21 ± 0.06	204.5 ± 5.6	117 / 2000	13 ± 4	169.5 ± 10.5 (7.5)
PdLII-7	8	3.1	0.52 ± 0.03	0.59 ± 0.03	0.01	1.16 ± 0.06	183.2 ± 6.4	87 / 2000	20 ± 4	158.6 ± 10.5 (7.3)
PdLII-15	9	2.8	0.52 ± 0.04	0.53 ± 0.03	0.01	1.09 ± 0.07	179.9 ± 13.0	34 / 1000	33 ± 6	165.2 ± 16.1 (13.7)

Table 3: Dose rate data, equivalent doses and OSL ages for sediment samples from Pech-de-l'Azé II.

Sample code	Layer	Moisture content (%)	Dose rates (Gy/ka)			Total dose rate (Gy/ka)	D_e (Gy)	Number of grains	Over-dispersion (%)	OSL age (ka)	*p*-value
			Beta	Gamma	Cosmic						
PdLIV-27	3A	3.8	0.57 ± 0.03	0.45 ± 0.02	0.12	1.17 ± 0.06	61.1 ± 1.7	112 / 2000	18 ± 3	52.4 ± 3.2 (2.5)	
PdLIV-26	3A	3.2	0.64 ± 0.04	0.44 ± 0.02	0.12	1.23 ± 0.07	60.3 ± 1.9	109 / 2000	24 ± 3	49.2 ± 3.2 (2.6)	
PdLIV-25	3A	4.7	0.53 ± 0.05	0.43 ± 0.02	0.12	1.10 ± 0.06	55.1 ± 1.8	108 / 2000	31 ± 3	49.9 ± 3.4 (2.9)	
PdLIV-24	3A	3.6	0.50 ± 0.03	0.42 ± 0.02	0.12	1.06 ± 0.06	57.3 ± 2.8	91 / 2000	38 ± 4	53.8 ± 4.0 (3.4)	
								Weighted mean =		***51.1 ± 2.4*** *(1.4)*	*p* = 0.65
PdLIV-23	3B	2.5	0.67 ± 0.04	0.40 ± 0.02	0.11	1.21 ± 0.06	59.7 ± 2.1	104 / 2000	26 ± 3	49.5 ± 3.2 (2.5)	
PdLIV-22	3B	3.5	0.62 ± 0.04	0.39 ± 0.02	0.11	1.15 ± 0.06	60.4 ± 2.1	101 / 2000	25 ± 3	52.5 ± 3.4 (2.7)	
PdLIV-21	3B	5.6	0.72 ± 0.05	0.39 ± 0.02	0.10	1.24 ± 0.08	64.0 ± 2.2	78 / 2000	29 ± 4	51.5 ± 3.8 (3.2)	
								Weighted mean =		***51.0 ± 2.6*** *(1.6)*	*p* = 0.71
PdLIV-20	4A	3.9	0.78 ± 0.04	0.46 ± 0.02	0.10	1.37 ± 0.07	72.6 ± 3.2	99 / 2000	34 ± 5	52.9 ± 3.7 (3.0)	
PdLIV-19	4A	3.4	0.89 ± 0.06	0.53 ± 0.03	0.10	1.54 ± 0.09	88.1 ± 3.5	92 / 1900	34 ± 4	57.1 ± 4.1 (3.5)	
PdLIV-18	4A	4.0	0.88 ± 0.05	0.58 ± 0.03	0.10	1.59 ± 0.08	90.3 ± 4.1	66 / 2000	26 ± 4	56.9 ± 4.0 (3.3)	
PdAIV-3	4A	4.0	0.84 ± 0.03	0.58 ± 0.03	0.10	1.56 ± 0.08	96.5 ± 4.8	70 / 2600	34 ± 4	61.8 ± 4.7 (3.9)	
PdLIV-17	4A	4.2	0.90 ± 0.05	0.51 ± 0.03	0.10	1.54 ± 0.08	92.8 ± 4.6	62 / 3000	28 ± 5	60.4 ± 4.4 (3.6)	
								Weighted mean =		***57.3 ± 2.8*** *(1.5)*	*p* = 0.40
PdLIV-16	4B	4.7	0.85 ± 0.05	0.45 ± 0.02	0.10	1.42 ± 0.07	87.5 ± 4.1	52 / 3000	19 ± 5	61.6 ± 4.4 (3.5)	
PdLIV-15	4B	6.8	0.83 ± 0.05	0.42 ± 0.02	0.09	1.38 ± 0.07	83.1 ± 3.3	87 / 2000	31 ± 4	60.4 ± 4.2 (3.3)	
PdLIV-14	4B	5.8	0.84 ± 0.05	0.40 ± 0.02	0.09	1.37 ± 0.07	86.5 ± 4.4	74 / 2000	34 ± 4	63.1 ± 4.8 (3.9)	
								Weighted mean =		***61.5 ± 3.4*** *(2.1)*	*p* = 0.87
PdLIV-13	4C	7.5	0.73 ± 0.05	0.38 ± 0.02	0.09	1.23 ± 0.08	81.1 ± 3.6	46 / 3000	17 ± 5	65.9 ± 5.2 (4.4)	
PdLIV-12	4C	5.4	0.53 ± 0.03	0.38 ± 0.02	0.09	1.03 ± 0.06	74.7± 4.0	47 / 2000	33 ± 6	72.4 ± 5.6 (4.8)	
PdLIV-11	4C	8.6	0.64 ± 0.04	0.37 ± 0.02	0.09	1.13 ± 0.07	75.8 ± 4.0	72 / 2000	36 ± 4	67.1 ± 5.4 (4.6)	
								Weighted mean =		***68.3 ± 3.9*** *(2.7)*	*p* = 0.57
PdLIV-10	5A	8.9	0.50 ± 0.03	0.37 ± 0.02	0.08	0.99 ± 0.06	76.5 ± 3.5	48 / 3000	19 ± 5	77.5 ± 6.0 (5.2)	
PdLIV-9	5A	9.1	0.53 ± 0.03	0.36 ± 0.02	0.08	1.01 ± 0.06	70.6 ± 2.7	108 / 2000	31 ± 3	74.3 ± 5.3 (4.2)	
PdLIV-8	5B/A	6.6	0.49 ± 0.04	0.39 ± 0.03	0.08	0.99 ± 0.06	77.1 ± 3.1	94 / 3000	38 ± 4	77.7 ± 5.7 (4.9)	
PdAIV-2	5B	6.6	0.46 ± 0.03	0.39 ± 0.03	0.08	0.97 ± 0.05	74.5 ± 7.3	39 / 2000	49 ± 8	77.2 ± 8.9 (8.4)	
								Weighted mean =		***76.3 ± 4.0*** *(2.6)*	*p* = 0.94
PdLIV-7	6A	7.8	0.61 ± 0.05	0.42 ± 0.02	0.08	1.14 ± 0.07	88.2 ± 2.6	106 / 2000	27 ± 3	77.2 ± 5.6 (4.6)	
PdLIV-6	6A	8.1	0.60 ± 0.04	0.41 ± 0.02	0.08	1.13 ± 0.07	83.5 ± 3.6	81 / 2000	31 ± 4	74.1 ± 5.6 (4.7)	
PdLIV-5	6B/A	7.1	0.56 ± 0.03	0.41 ± 0.02	0.07	1.07 ± 0.06	82.4 ± 2.9	114 / 2000	28 ± 3	77.0 ± 5.3 (4.2)	
PdLIV-4	6B	8.9	0.57 ± 0.04	0.35 ± 0.02	0.07	1.02 ± 0.06	77.8 ± 3.4	83 / 2000	30 ± 4	76.3 ± 5.7 (4.8)	
PdLIV-3	6B	9.3	0.41 ± 0.03	0.35 ± 0.02	0.07	0.86 ± 0.06	68.3 ± 2.5	115 / 2000	31 ± 3	79.8 ± 6.1 (5.3)	
								Weighted mean =		***76.7 ± 3.7*** *(2.1)*	*p* = 0.99
PdAIV-1-A	8	5.6	0.27 ± 0.03	0.24 ± 0.01	0.05	0.60 ± 0.04	55.1 ± 2.7	90 / 1000	39 ± 4	91.5 ± 7.6 (7.1)	
PdLIV-2	8	5.6	0.23 ± 0.03	0.33 ± 0.02	0.05	0.65 ± 0.05	62.7 ± 1.6	142 / 1000	22 ± 3	97.4 ± 7.6 (6.9)	
PdAIV-1-B	8	5.6	0.23 ± 0.03	0.33 ± 0.02	0.05	0.64 ± 0.05	63.5 ± 4.5	80 / 1500	72 ± 6	98.6 ± 11.1 (10.7)	
PdAIV-1-C	8	6.9	0.29 ± 0.03	0.31 ± 0.02	0.05	0.69 ± 0.05	62.9 ± 3.6	89 / 1000	48 ± 4	91.6 ± 8.8 (8.2)	
PdAIV-1-D	8	8.1	0.31 ± 0.02	0.29 ± 0.02	0.05	0.68 ± 0.04	66.6 ± 2.3	171 / 2000	38 ± 3	97.4 ± 7.4 (6.3)	
PdLIV-1	8	8.1	0.41 ± 0.03	0.29 ± 0.02	0.05	0.79 ± 0.05	73.9 ± 2.2	112 / 1000	23 ± 2	93.8 ± 6.7 (5.6)	
								Weighted mean =		***94.8 ± 4.3*** *(2.9)*	*p* = 0.95

Table 4: Dose rate data, equivalent doses and OSL ages for sediment samples from Pech-de-l'Aze IV. See Table 2 for explanation of *p*-value.

Climatic Phase	Pech I		Pech II		Pech IV		
Würm / Périgord	Layer	Industry	Layer	Industry	Layer (Bordes, 1975)	Layer (Turq et al., 2011)	Industry
II / V (less cold, damp)	Rock fall	—	—	—	E	1	—
II/ IV (very cold, dry)	7	MTA-B	—	—	F1	2	
II / III (less cold, damper)	6	MTA-B	—	—	F2	3A	MTA-B
II / II (cold, dry)	5	MTA-A/B	—	—	F3	3A	MTA-A/B
II / I (very cold, damp)	4	MTA-A	—	—	F4	3B	MTA-A
I / IX (cold, very dry)	—	—	2A–2C	Mousterian	G	4A	Mousterian
I / VIII (milder)	—	—	2D	Mousterian	H1–H2	4A	TM?
I / VII (cold, dry)	—	—	2E–2F	TM	I1–I2	4B (I1)	TM
						4C (I2)	
I / VI (mild)	—	—	2G	Mousterian	J1	5A	TM?
I / V (short, cold)	—	—	2G’ top	Mousterian	J2	5B	TM?
I / IV (mild, damp)	—	—	2G’ base	Mousterian	J3a–c	6A (J3a-b)	Asinipodian
						6B (J3c)	
I / III (cold, dry)	—	—	3	TM	Rock fall		—
I / II (mild, damp)	—	—	4A	TM	X	7 (X top)	TM
	—	—	4B	DM	X		TM
	—	—	4C	TM	X		TM
I / I (short, cold)	—	—	4D–E	TM	Y–Z	8 (X base, Y-Z)	TM

Table 5: Correlations between the three sites proposed by Bordes (1975, 1978) based on the climate, fauna, geology and archaeological industries. Also shown for Pech IV is the current stratigraphic units proposed in Turq et al. (2011) and used in the rest of this study. MTA – Mousterian of the Acheulian Tradition; TM – Typical Mousterian; DM – Denticulate Mousterian.

Climatic Phase	Pech I		Pech II		Pech IV	
Marine Isotope Stage (MIS) / Approximate age	Layer	Industry	Layer	Industry	Layer	Industry
	Rock fall	—			1	—
MIS 3 (~51 ka)	7 6 5 4	MTA-B MTA-B MTA-A/B MTA-A			2 3A 3A 3B	MTA with trends consistent with Type A to B change
End of MIS 4, beginning of MIS 3 (~63 to ~55 ka)			2A–2G 3 4A	FM with Levallois flakes and Quina scrapers TM TM	4A 4B (I1)	High scraper percentages, high but decreasing Levallois TM with likely Quina at the top
End of MIS 5a, all of MIS 4 (~77 to ~65 ka)					4C 5A 5B	TM - High Scrapers and Levallois
					6A 6B	Low Scrapers, increasing Levallois, Asinipodian
MIS 5d to MIS 5b (~105 to ~80 ka)			4B	DM		
			4C	TM	7	?
			4D–E		8	TM - High scrapers with some Levallois
MIS6 (~180-~140 ka)			6-9	Clactonian and Acheulian		

Table 6: Correlations between the three Pech sites based on the chronologies constructed in this study, together with the broad age range and corresponding marine isotope stages. MTA – Mousterian of the Acheulian Tradition; TM – Typical Mousterian; DM – Denticulate Mousterian.

Figure 1

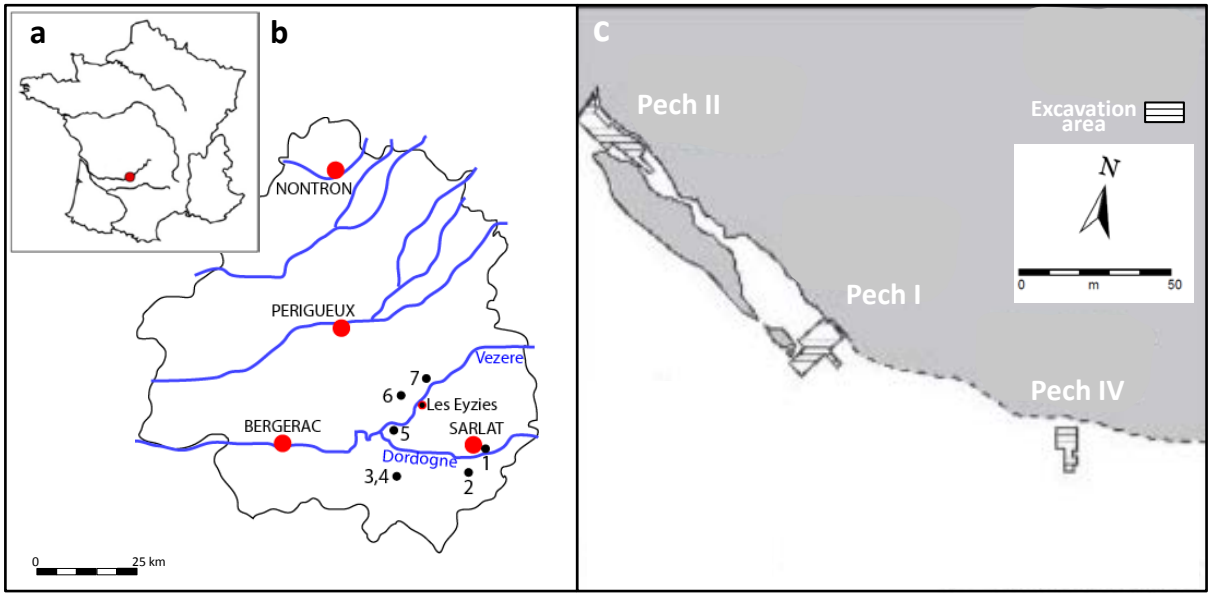
a
b
NONTRON
PERIGUEUX
Vezere
7
6
Les Eyzies
5
BERGERAC
SARLAT
Dordogne
1
2
3,4
0
25 km
C
Pech II
Excavation area
N
0
m
50
Pech I
Pech IV

Figure 2

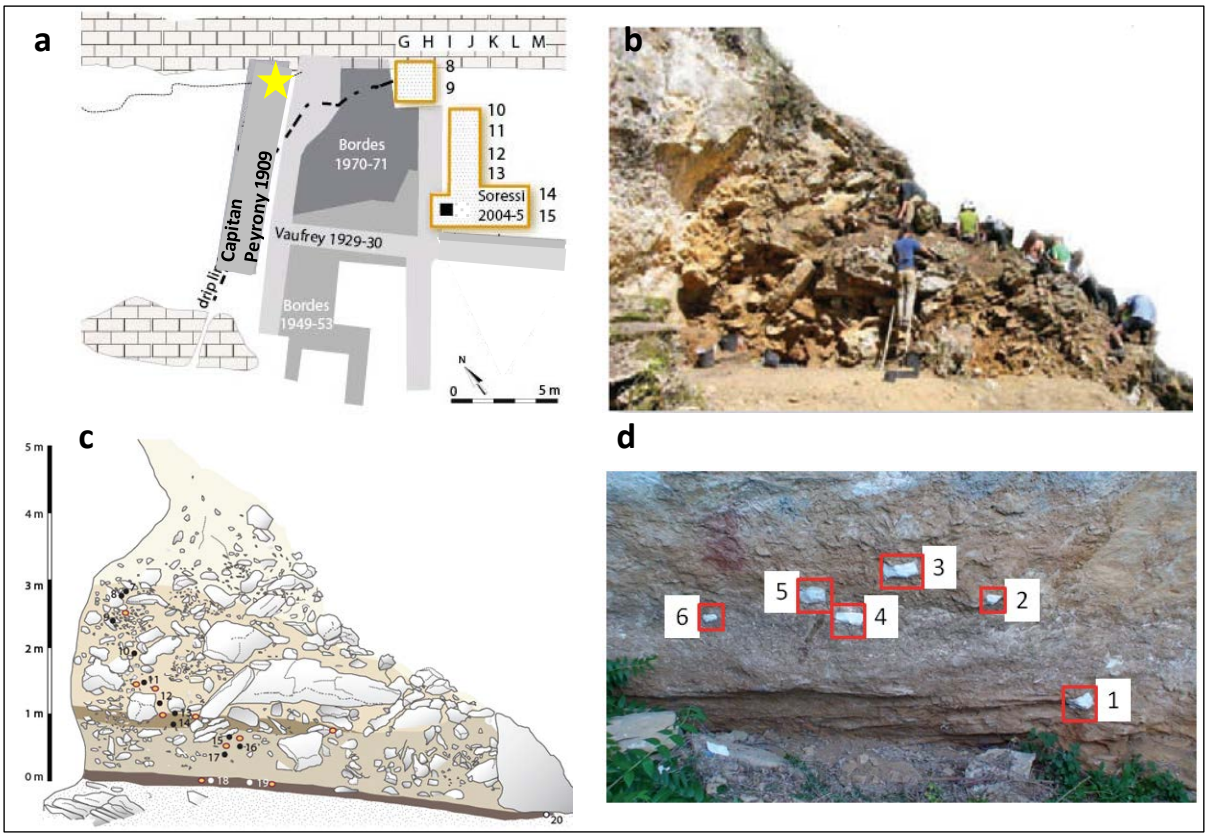
a
G H I J K L M
8
9
10
11
12
13
14
15
Bordes
1970-71
Soressi
2004-5
Capitan
Peyrony 1909
Vaufrey 1929-30
Bordes
1949-53
drip line
N
0
5 m
b
c
5 m
4 m
3 m
2 m
1 m
0 m
d
1
2
3
4
5
6

Figure 3

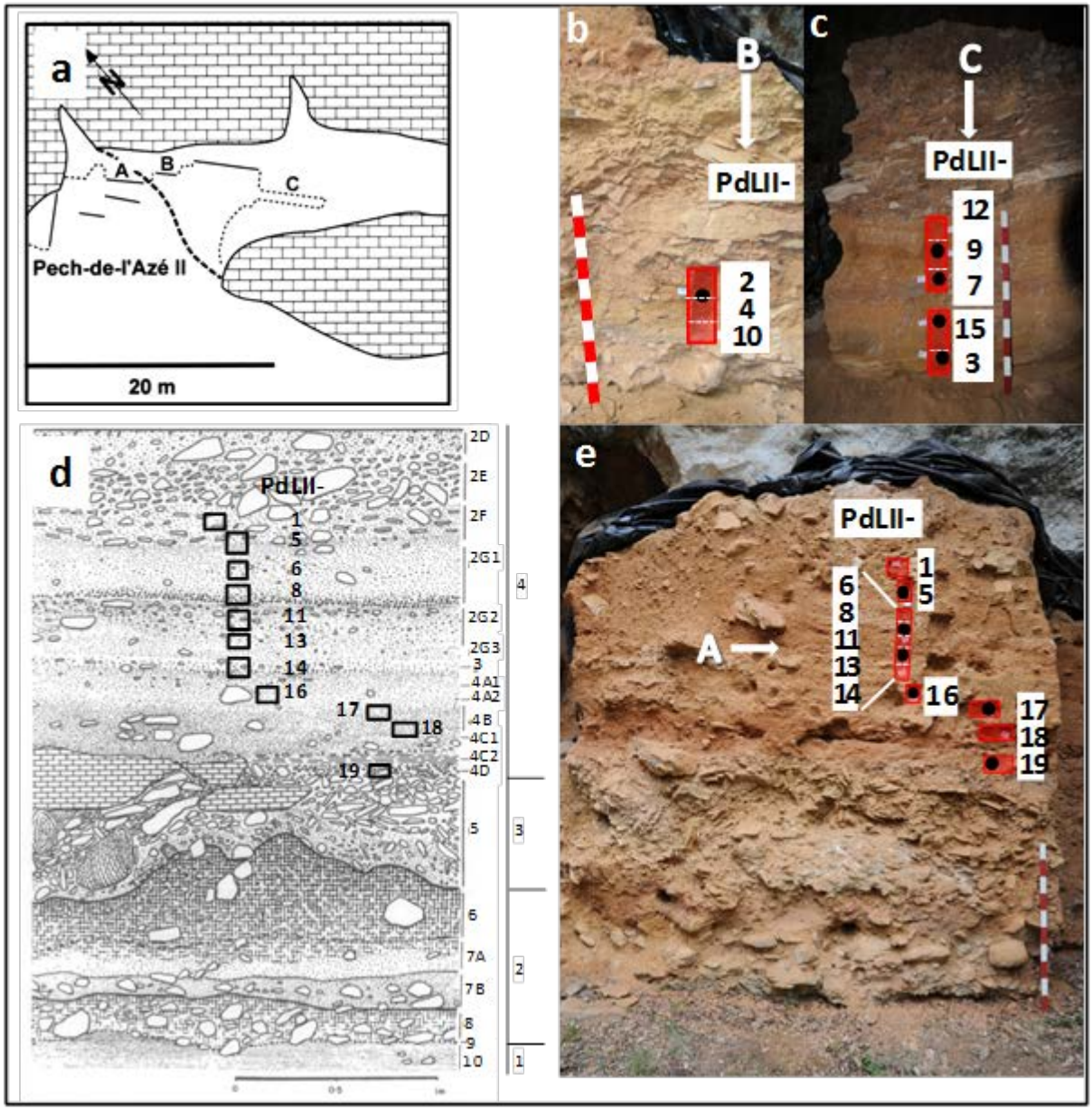
a
A
B
C
Pech-de-l'Azé II
20 m
b
B
PdLII-
2
4
10
c
C
PdLII-
12
9
7
15
3
d
PdLII-
1
5
6
8
11
13
14
16
17
18
19
2D
2E
2F
2G1
2G2
2G3
3
4A1
4A2
4B
4C1
4C2
4D
5
6
7A
7B
8
9
10
4
3
2
1
e
PdLII-
A
1
5
6
8
11
13
14
16
17
18
19

Figure 4

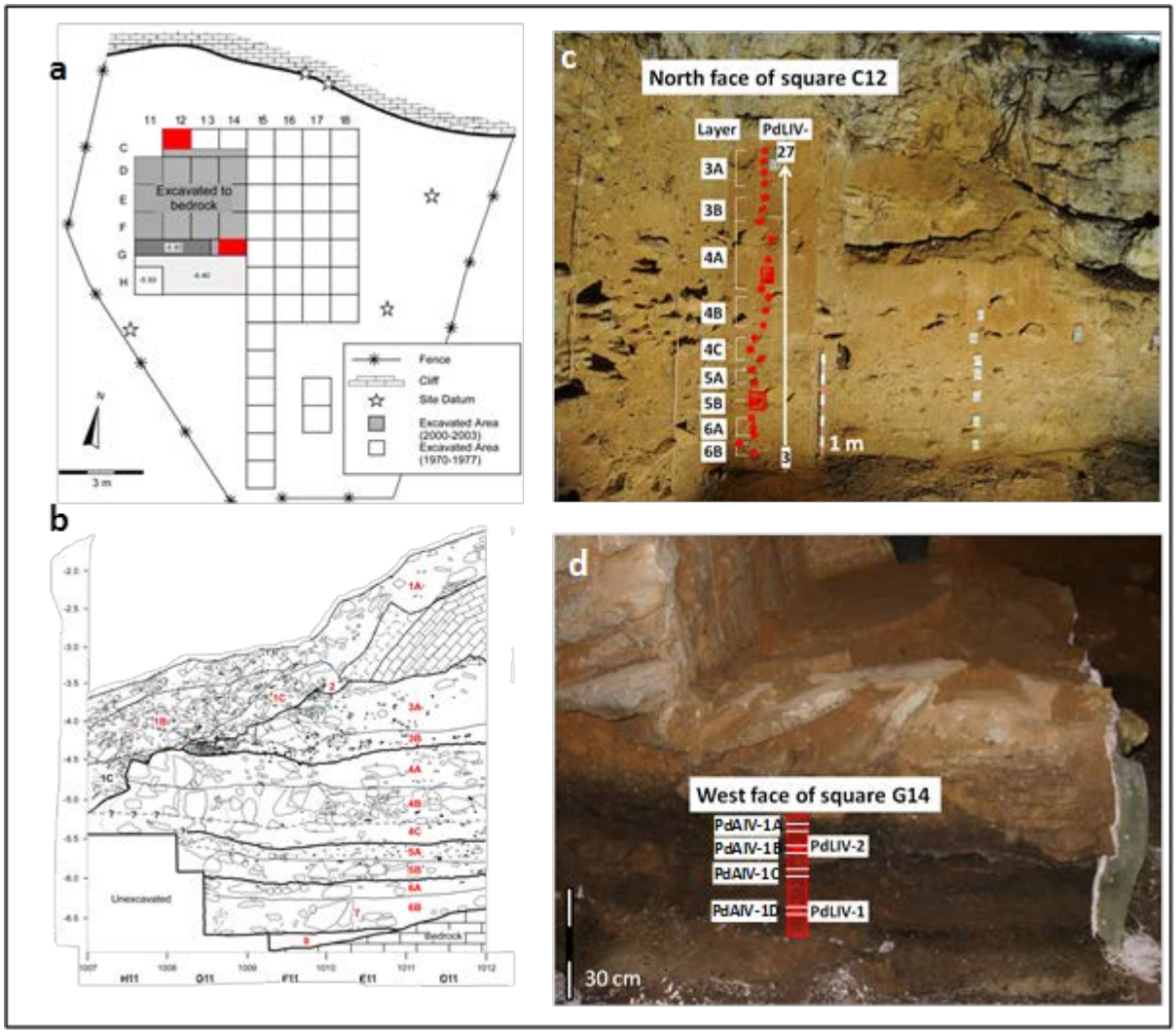
a
Excavated to bedrock
Fence
Cliff
Site Datum
Excavated Area (2000-2003)
Excavated Area (1970-1977)
3 m
b
Unexcavated
Bedrock
c
North face of square C12
Layer
PdLIV-27
3A
3B
4A
4B
4C
5A
5B
6A
6B
1 m
d
West face of square G14
PdAIV-1A
PdAIV-1B
PdAIV-1C
PdAIV-1D
PdLIV-2
PdLIV-1
30 cm

Figure 5

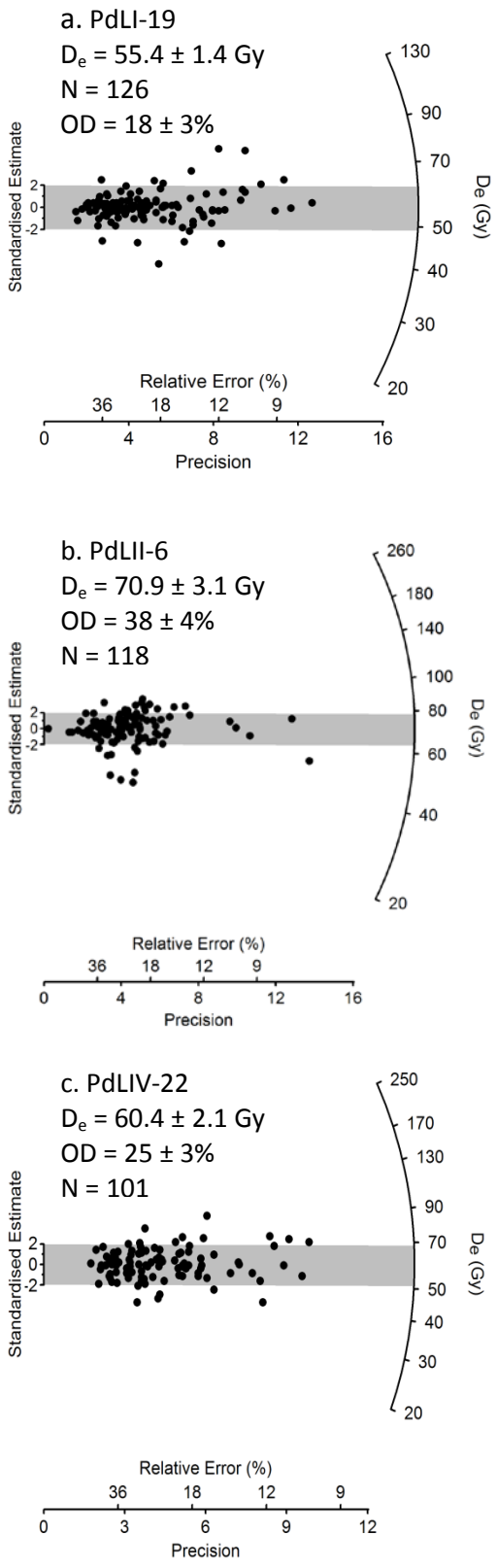
a. PdLI-19
De = 55.4 ± 1.4 Gy
N = 126
OD = 18 ± 3%
Standardised Estimate
De (Gy)
Relative Error (%)
Precision
b. PdLII-6
De = 70.9 ± 3.1 Gy
OD = 38 ± 4%
N = 118
c. PdLIV-22
De = 60.4 ± 2.1 Gy
OD = 25 ± 3%
N = 101

Figure 6

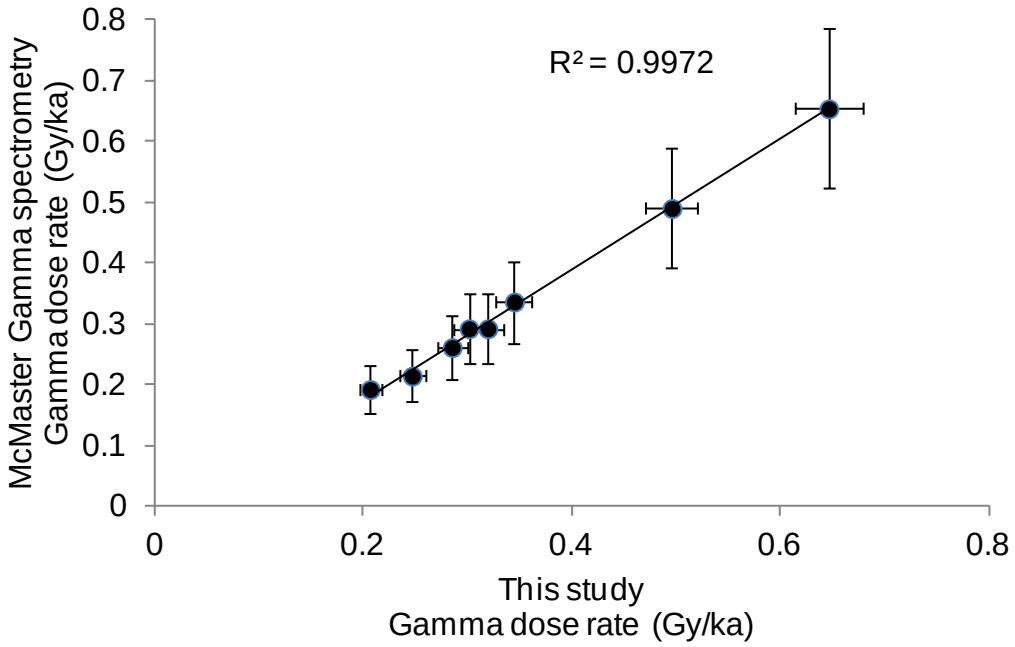
R² = 0.9972
McMaster Gamma spectrometry
Gamma dose rate (Gy/ka)
This study
Gamma dose rate (Gy/ka)
0
0.1
0.2
0.3
0.4
0.5
0.6
0.7
0.8
0
0.2
0.4
0.6
0.8

Figure 7

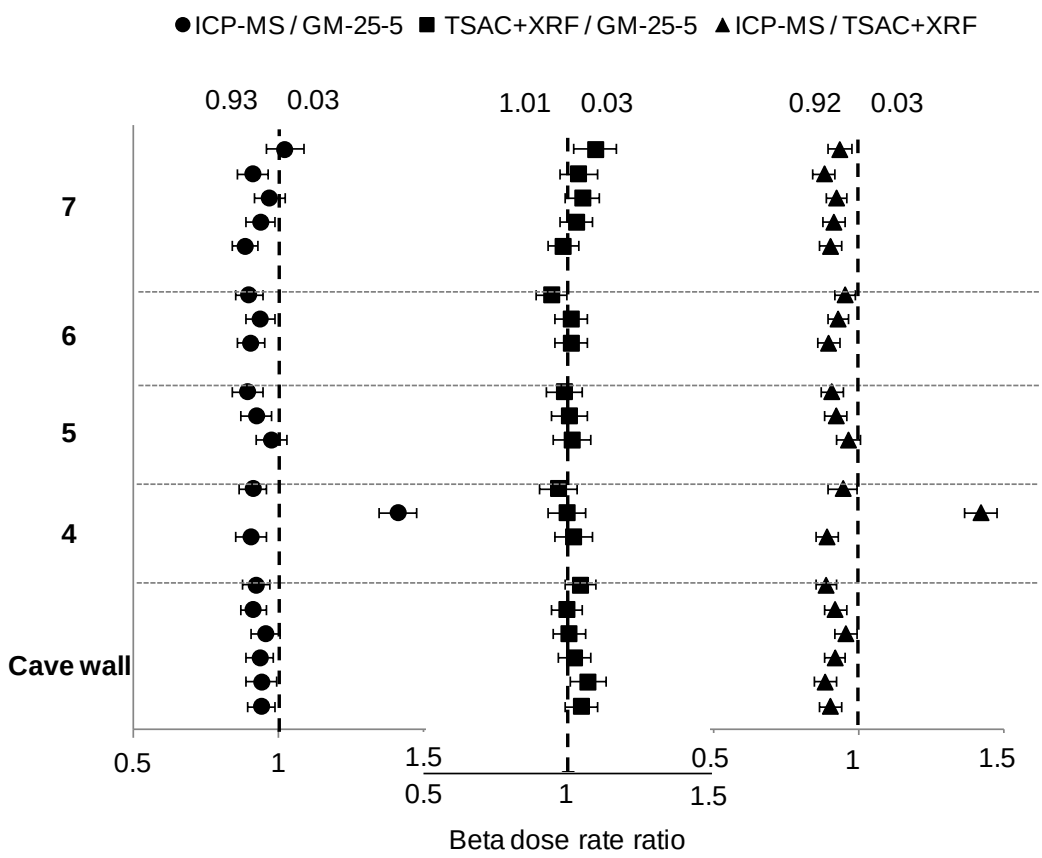
ICP-MS / GM-25-5
TSAC+XRF / GM-25-5
ICP-MS / TSAC+XRF
0.93 0.03
1.01 0.03
0.92 0.03
7
6
5
4
Cave wall
0.5
1
1.5
0.5
1
1.5
0.5
1
1.5
Beta dose rate ratio

Figure 8

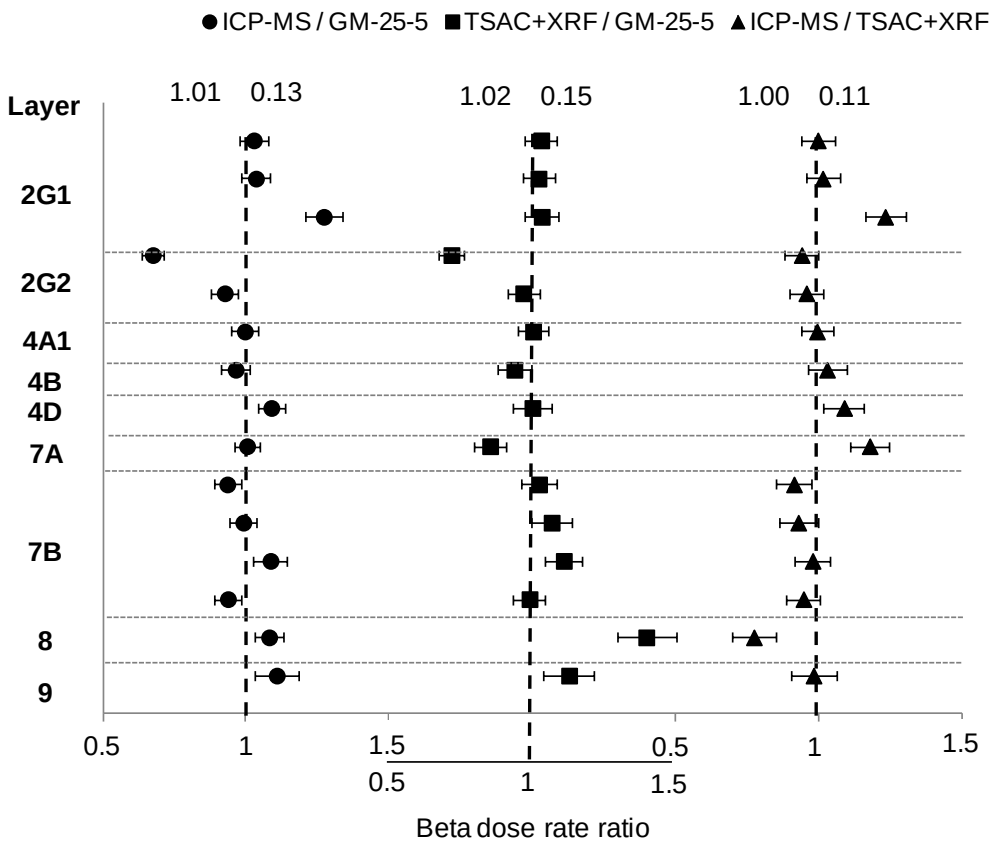
ICP-MS / GM-25-5
TSAC+XRF / GM-25-5
ICP-MS / TSAC+XRF
Layer
1.01
0.13
1.02
0.15
1.00
0.11
2G1
2G2
4A1
4B
4D
7A
7B
8
9
0.5
1
1.5
0.5
1
1.5
0.5
1
1.5
Beta dose rate ratio

Figure 9

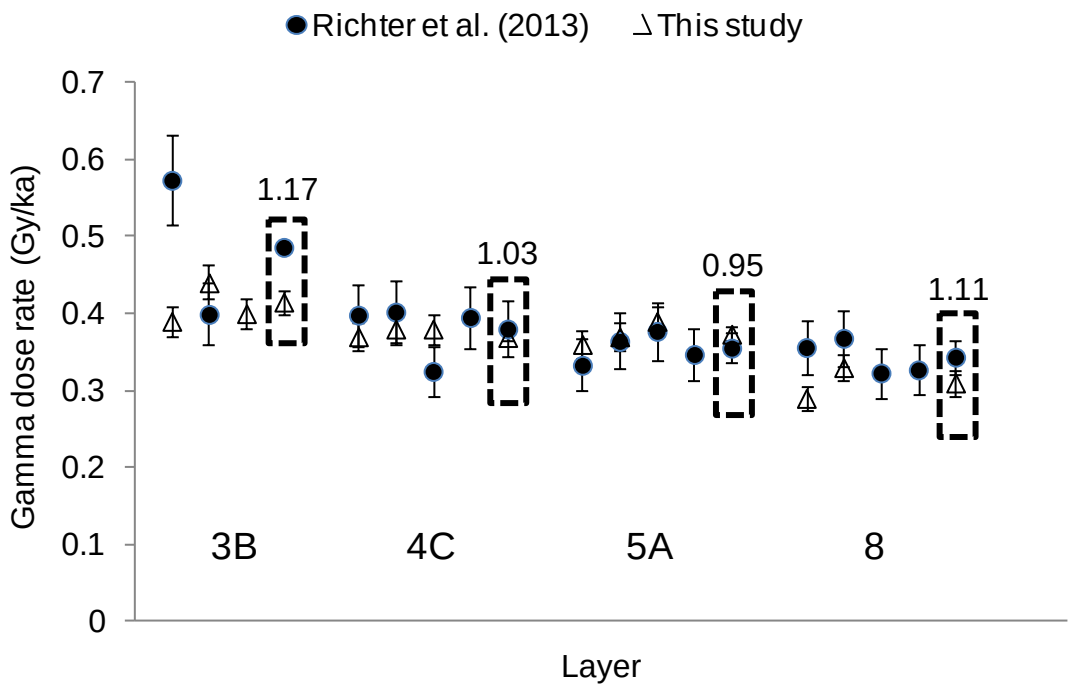
Richter et al. (2013)
This study
Gamma dose rate (Gy/ka)
0.7
0.6
0.5
0.4
0.3
0.2
0.1
0
1.17
1.03
0.95
1.11
3B
4C
5A
8
Layer

Figure 10

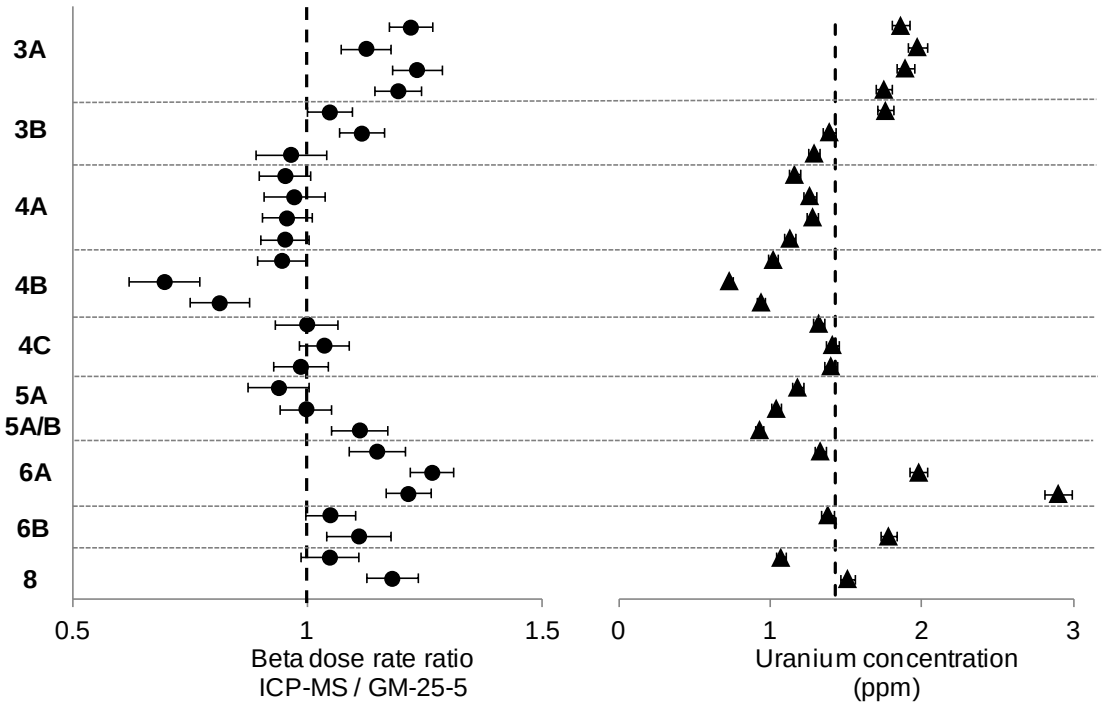
3A
3B
4A
4B
4C
5A
5A/B
6A
6B
8
0.5
1
1.5
Beta dose rate ratio
ICP-MS / GM-25-5
0
1
2
3
Uranium concentration
(ppm)

Figure 11

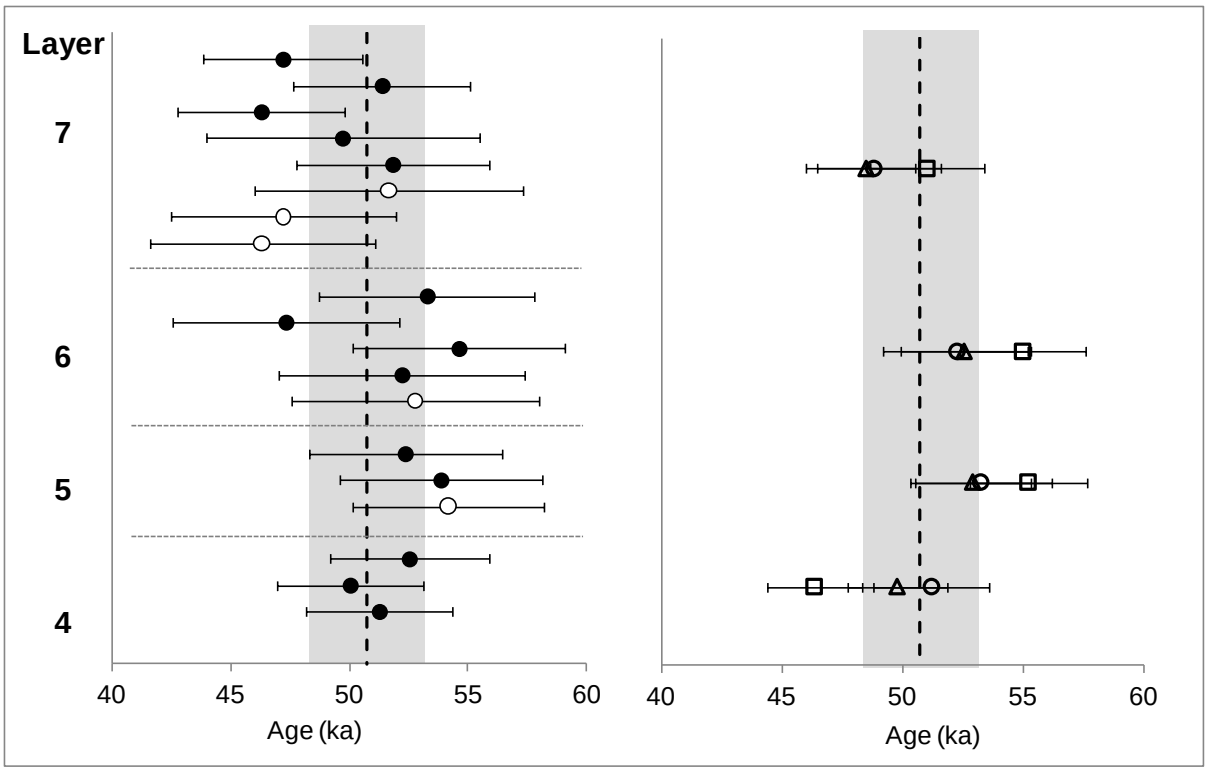

Figure 12

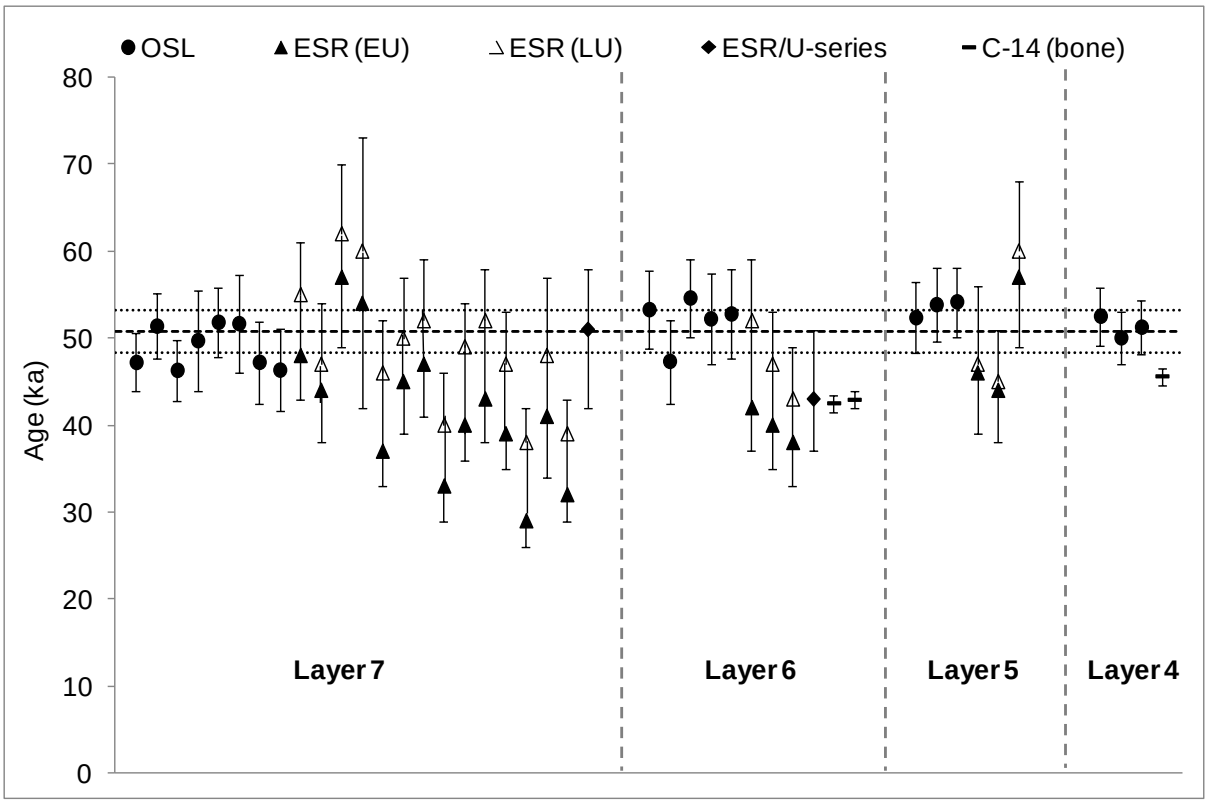
OSL
ESR (EU)
ESR (LU)
ESR/U-series
C-14 (bone)
Age (ka)
80
70
60
50
40
30
20
10
0
Layer 7
Layer 6
Layer 5
Layer 4

Figure 13

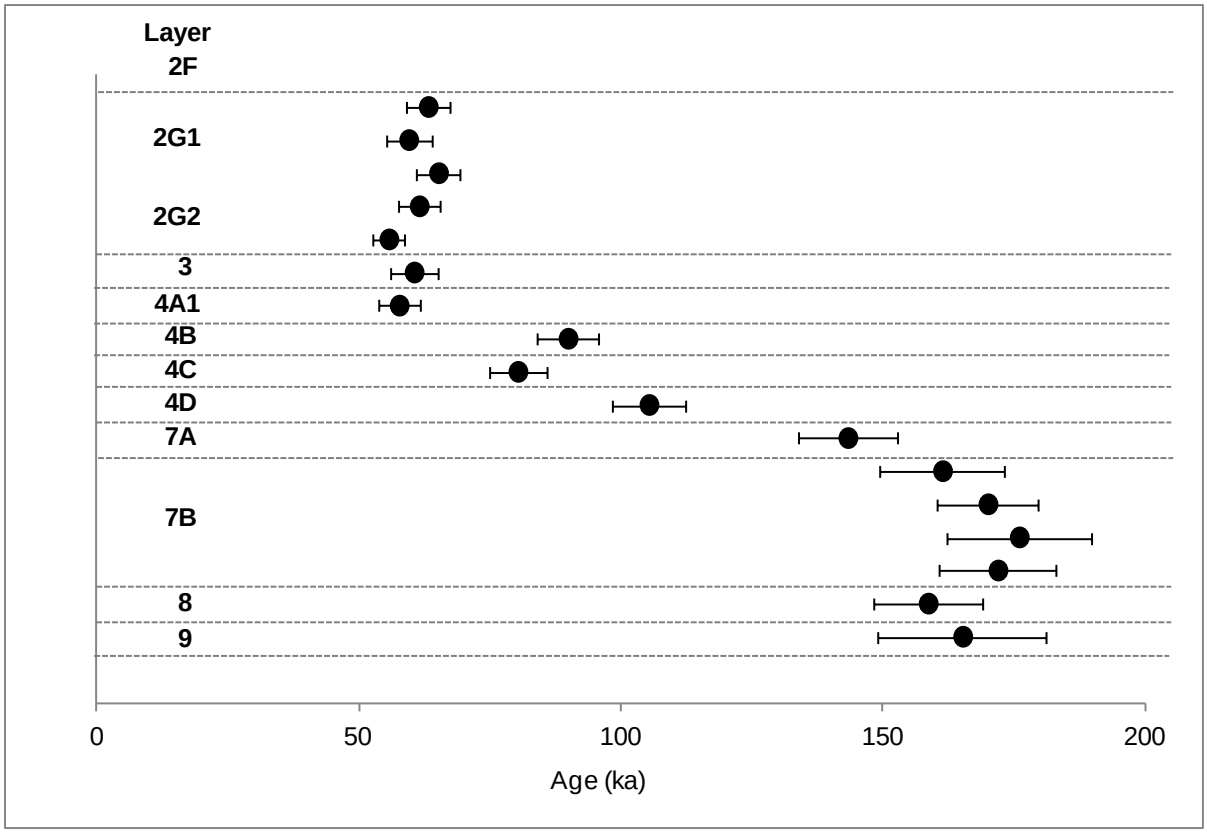

Figure 14

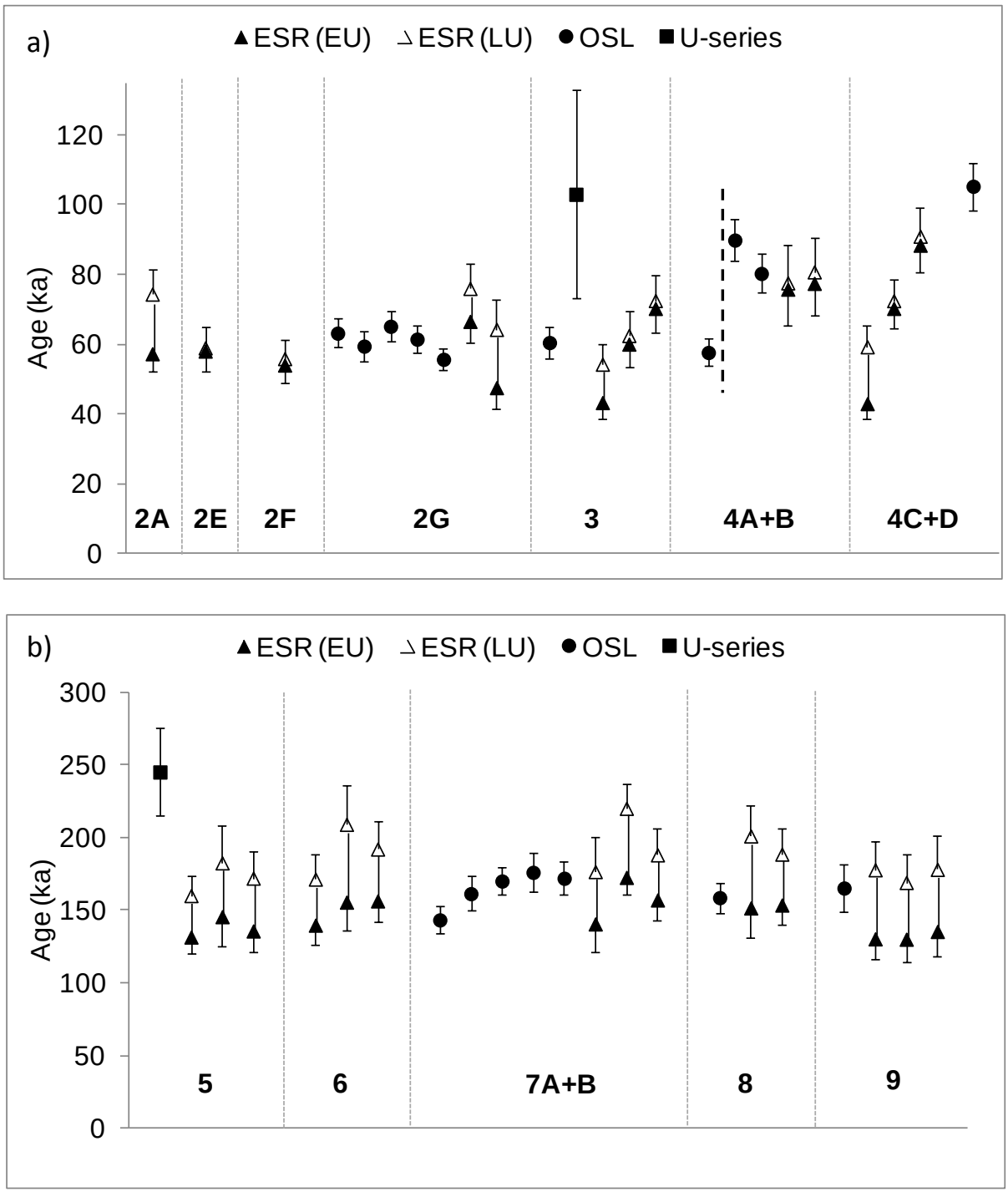
a)
ESR (EU)
ESR (LU)
OSL
U-series
Age (ka)
0
20
40
60
80
100
120
2A
2E
2F
2G
3
4A+B
4C+D
b)
ESR (EU)
ESR (LU)
OSL
U-series
Age (ka)
0
50
100
150
200
250
300
5
6
7A+B
8
9

Figure 15

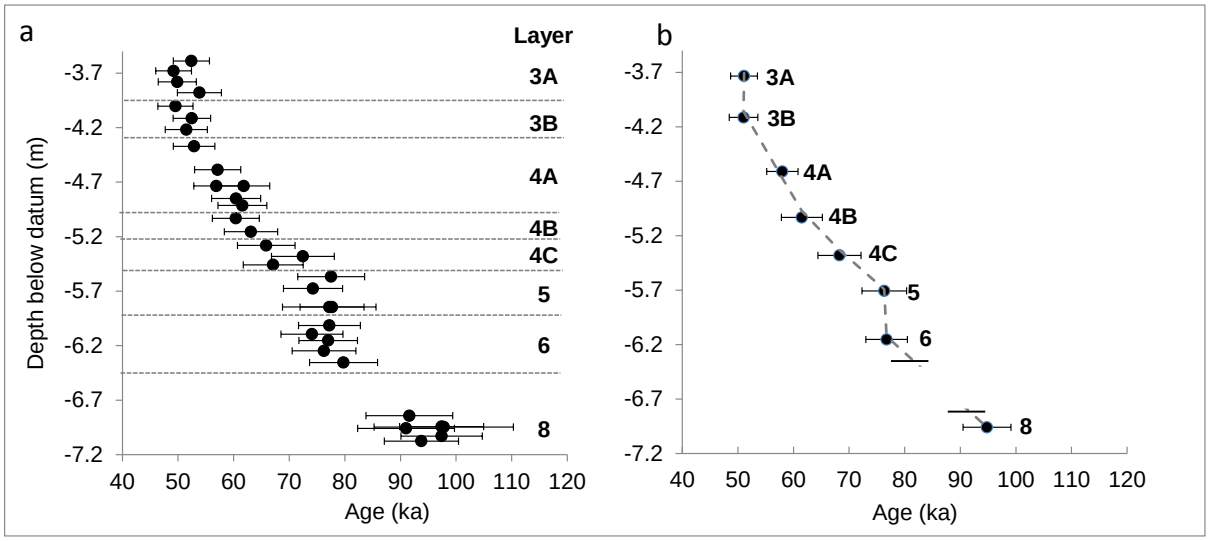
a
Layer
3A
3B
4A
4B
4C
5
6
8
Depth below datum (m)
-3.7
-4.2
-4.7
-5.2
-5.7
-6.2
-6.7
-7.2
40
50
60
70
80
90
100
110
120
Age (ka)
b
3A
3B
4A
4B
4C
5
6
8
Age (ka)

Figure 16

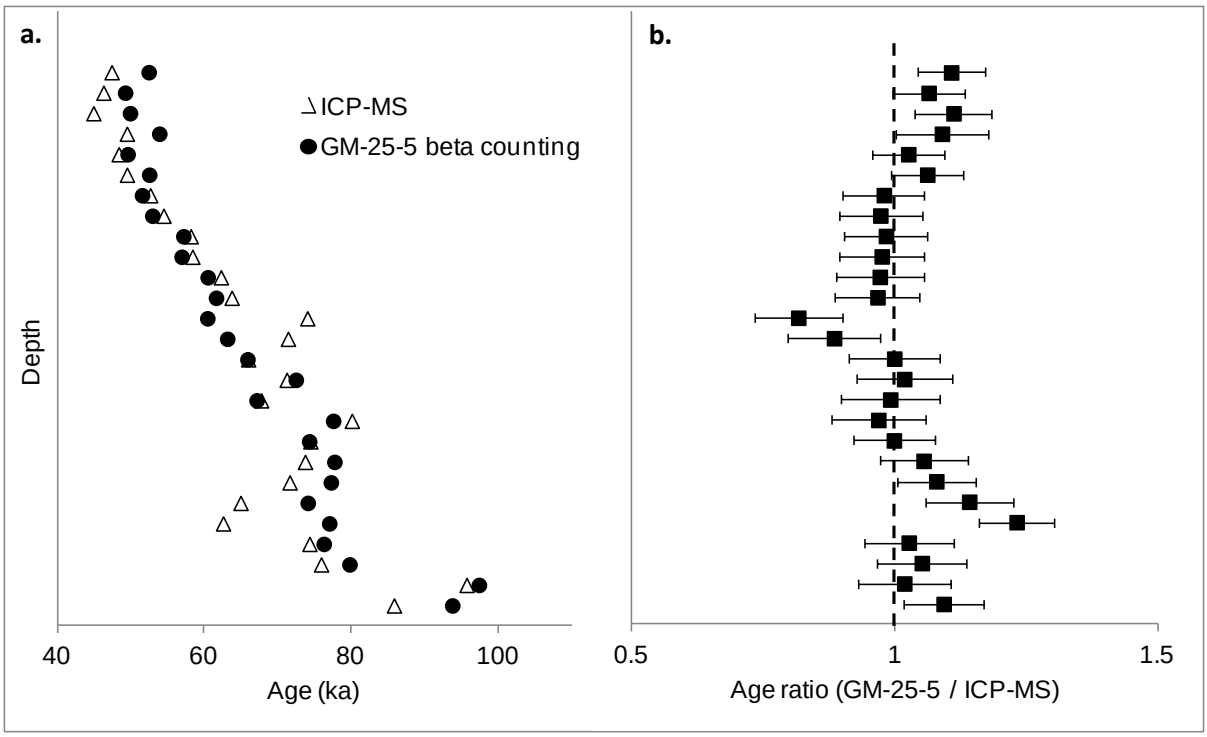
a.
ICP-MS
GM-25-5 beta counting
Depth
40
60
80
100
Age (ka)
b.
0.5
1
1.5
Age ratio (GM-25-5 / ICP-MS)

Figure 17

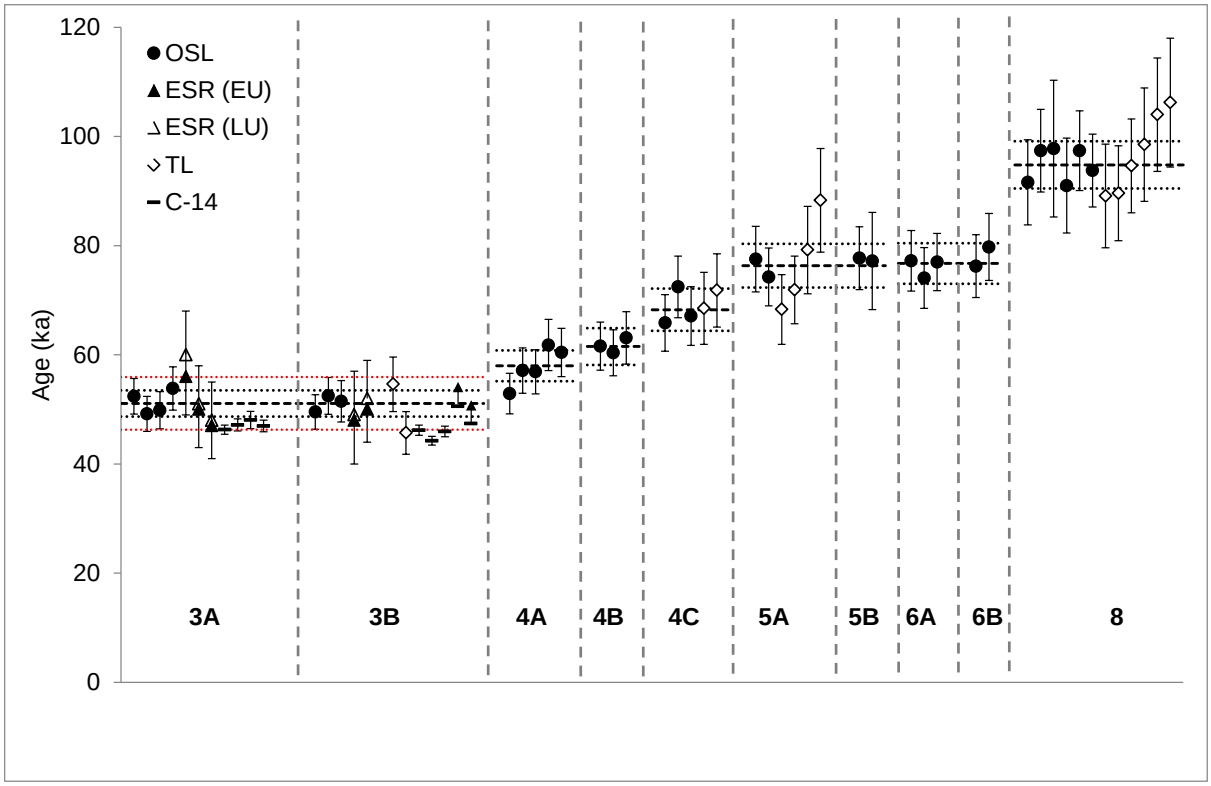
120
100
80
60
40
20
0
Age (ka)
OSL
ESR (EU)
ESR (LU)
TL
C-14
3A
3B
4A
4B
4C
5A
5B
6A
6B
8

Figure 18

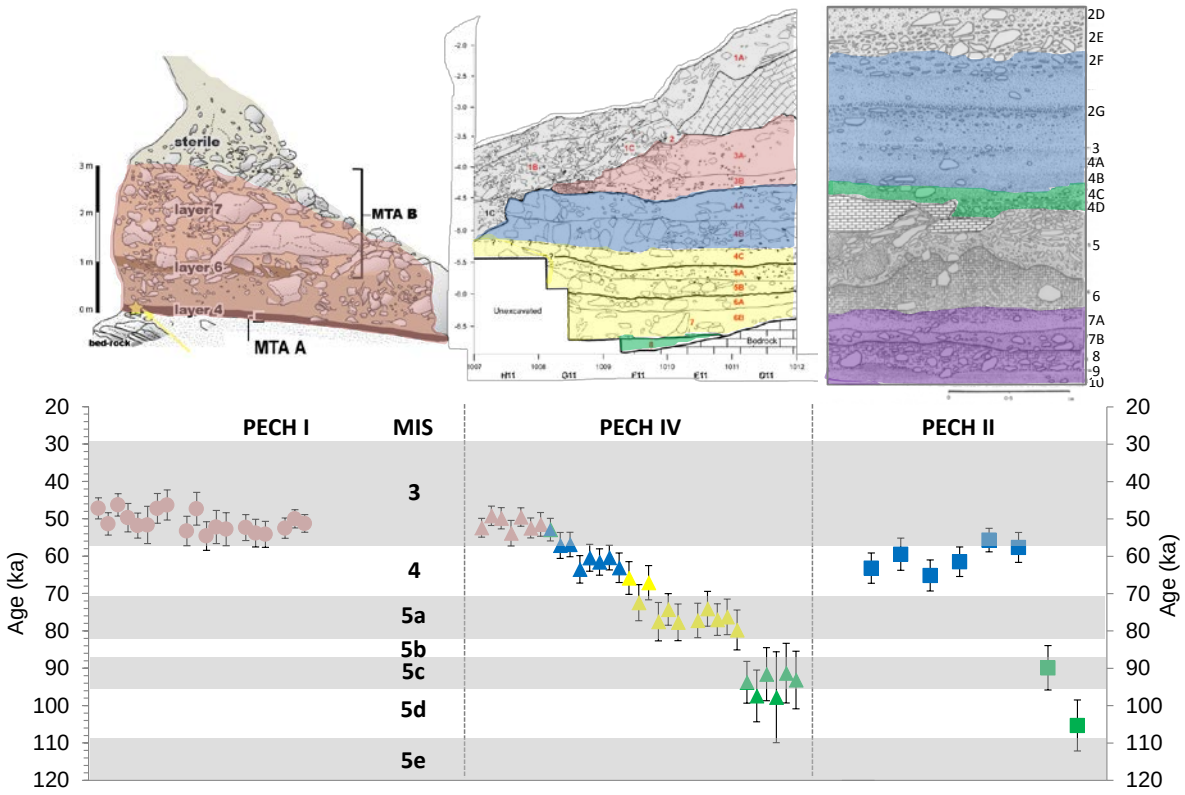
sterile
layer.7
layer.6
layer.4
bed-rock
MTA B
MTA A
Unexcavated
Bedrock
2D
2E
2F
2G
3
4A
4B
4C
4D
5
6
7A
7B
8
9
10
PECH I
MIS
PECH IV
PECH II
3
4
5a
5b
5c
5d
5e
Age (ka)
20
30
40
50
60
70
80
90
100
110
120

Supplementary Material

Click here to download Supplementary Material: Paper II - Supplementary information (after revision)_CH_ZJ.pdf